

# We are IntechOpen, the world's leading publisher of Open Access books Built by scientists, for scientists

5,300

Open access books available

130,000

International authors and editors

155M

Downloads

Our authors are among the

154

Countries delivered to

TOP 1%

most cited scientists

12.2%

Contributors from top 500 universities



WEB OF SCIENCE™

Selection of our books indexed in the Book Citation Index  
in Web of Science™ Core Collection (BKCI)

Interested in publishing with us?  
Contact [book.department@intechopen.com](mailto:book.department@intechopen.com)

Numbers displayed above are based on latest data collected.  
For more information visit [www.intechopen.com](http://www.intechopen.com)



---

# Opportunities of Scanning Probe Microscopy for Electrical, Mechanical and Electromechanical Research of Semiconductor Nanowires

---

Pavel Geydt, Mikhail S. Dunaevskiy and Erkki Lähderanta

Additional information is available at the end of the chapter

<http://dx.doi.org/10.5772/intechopen.68162>

---

## Abstract

In this chapter, three types of phenomena (electrical, mechanical, and electromechanical) that can be investigated in individual III–V semiconductor nanowires with scanning probe microscope are presented. Transport measurements in GaAs nanowires based on stable electric connection provided opportunity to study individual vertical freestanding nanowires under gentle precisely controlled force. Latter approach appears superior to studies of horizontally fixed nanowires because studying vertical as-grown nanowires avoids charge leakage into the substrate and impact of defects caused by breakage of nanowires. Principles of thermionic emission theory are used to characterize electrical effects in individual as-grown nanowires. Effects of SiO<sub>2</sub> protective layer, surface passivation layers, illumination, and influence of sweeping rate of current-voltage recording are analyzed. Elastic studies are performed for individual InP nanowires affixed at one end. Bending of the tapered nanowires with diameters of a narrow free end either 10 or 20 nm was performed under different loading forces. It allowed calculation of flexibility coefficient profiles along the nanowires' axes. Improved numerical model for tapered nanowires leads to the finding of Young's modulus of wurtzite InP material in nanowires. Piezoelectric measurements permitting registration of reverse piezo effect with opportunities of direct piezo response recording for individual wurtzite GaAs nanowires are briefly described.

**Keywords:** scanning probe microscopy, AFM, PFM, current-voltage characteristics, Young's modulus

---

## 1. Introduction

Recent technological challenges of nanotechnology and industry are lying in two main fields: characterization and production of nanostructures. In order to enhance the quality of nanodevices, it is vital to know properties of the nanostructures involved and specific features that are attributed to their scaling. Since nanowires (NWs) are one of the most prominent objects of nanoscience, significant attention is being paid to their properties and throughput investigation [1–7].

However, already choosing an appropriate method for studying NWs is hard due to their small size and fragility. NWs are quasi one-dimensional structures with nanoscale width possessing properties that dramatically change due to the size effects [8]. Diameter of NWs is approximately 10–100 nm with considerable value of length-to-diameter ratio. In addition, surface-to-volume ratio of NWs defines their strong dependence from the surface effects [1]. Typically, well-established massive methods of investigation are used to characterize the entire arrays of NWs [2, 5]: photoluminescence (PL), X-ray diffraction (XRD), scanning electron microscopy (SEM), transmission electron microscopy (TEM), optical methods, etc. All above-mentioned techniques have limitations on spatial resolution and type of information provided by each certain technique. Definitely, a precise and accurate method focused onto single-object study and revealing features of individual nanostructures should be proposed to support inductive reasoning over properties of NWs inside arrays. Furthermore, if properties of an individual object will be revealed in details, it seems achievable to tune the object's properties and then replicate improved structures into a regular array. Later, such "perfect" array of NWs can be used to create advanced devices based on NWs. Thus, detailed understanding of structure's parameters and its material's properties is expected to benefit innovative technologies. Nanowire-based devices already attract significant attention as units establishing new energy sources [3, 9–11], sensors [12–14], transistors [7, 15], NEMS [16, 17], etc.

Due to the challenges associated with NWs, a novel multifunctional helping hand needs to be utilized for their systematic study. Exactly scanning probe microscopy (SPM) as a family of research methods provides visualization, examination, and even changing of properties of individual nanostructures [18–20]. SPM-based methods were successfully performing this challenging role for NWs as reported previously [21–26]. For example, exactly SPMs are enthusiastically used in studies of new materials and assemblies in modern field of piezotronics [10, 27, 28]. However, description of prospects of electromechanical SPM methods for NWs seems not properly structured yet. Moreover, SPM is an intensively progressing tool, which regularly establishes new and enhanced opportunities for an advanced research [29–31]. We will try to represent accumulated knowledge and our experience in NWs and SPM to help in further studies of NWs. This is done with aspiration that adequate description of SPM methods will stimulate designing and R&D of NW-based devices. Thus, we will represent our results of studies of an individual III-V semiconductor NWs within an enhanced experimental methodology.

Primary issue in such work is establishing of classification under which a comprehensive study will be presented. Among different variants: (1) by composition of material used in NWs (GaAs, InP, GaN); (2) by microscopic method (force spectroscopy, quantitative nanomechanical mapping (QNM), conductive atomic force microscopy (C-AFM), Kelvin probe force microscopy (KPFM), piezoresponse force microscopy (PFM), etc.); (3) by geometrical orientation of the NWs (vertical,

horizontal, inclined, or stumps rest after breakage of NWs); and (4) by properties of interest; we preferred the latter class. Therefore, the chapter consists of three following sections: electrical, mechanical, and electromechanical properties of NWs and represents methods of their investigation by modern SPM approaches. Latter means that magnetic [32–35], optical [29, 36–39], acoustic [10, 40–45], catalytic [46], and other properties [47–49] will not be reflected in recent chapter due to format limitations but are proposed to be accessed from the denoted comprehensive works.

NWs described in Sections 2 and 3 were grown by vapor-liquid-solid (VLS) mechanism [4] in metaloxide vapor phase epitaxy (MOVPE) chamber. Catalytic golden droplets were sputtered on substrate under the temperature  $\sim 450^\circ\text{C}$  followed by the initiation of a volatile precursor's flow in a predefined protocol [50]. Diameters of NWs were  $\sim 100$  nm in accordance with width of the Au droplets. Lengths were controlled by duration of the precursor's flow:  $\sim 1$   $\mu\text{m}$  for vertical structures,  $\sim 5$   $\mu\text{m}$  for horizontal NWs, and  $\sim 3$   $\mu\text{m}$  for inclined NWs. NWs for electrical studies were highly p-doped ( $\sim 10^{19}$   $\text{cm}^{-3}$ ) by diethylzinc flow. Comprehensive details about fabrication setup and technique can be accessed from [50]. Samples with horizontal NWs in Section 2 were prepared by a procedure similar to the above described, although after fabrication, the NWs were broken from the substrate and dispersed in distilled water. Acquired suspension was placed onto clean  $\text{SiO}_2$  substrate. When water has evaporated, NWs appeared fixed to the substrate by adhesive force. This step was followed by optical lithography, which finally connected separate NWs into electric circuit connected with macro-sized electrodes. Circuiting has been initially checked by SEM and verified by SPM performed afterward. Inclined InP NWs were fabricated on silicon wafers without intentional doping to preserve the pure wurtzite crystal structure of InP.

Subsequent studies were carried out on standard SPM Multimode 8 (Bruker, USA) equipped with additional modules, e.g., either PeakForce KPFM or PeakForce TUNA [51]. Both regimes were accompanied by quantitative nanomechanical mapping (QNM). Separately, few types of spectroscopies were executed. This means that individual single-point-oriented studies were performed with SPM, e.g., force-distance spectroscopy  $F(z)$ , current-voltage spectroscopy (I–V curves), or current-time spectroscopy  $I(t)$ .

PFM studies presented in Section 4 were done for wurtzite GaAs NWs fabricated with molecular beam epitaxy (MBE) method (details can be found in [52]). Measurements were performed in standard protocol, where specific AC voltage (frequency  $\sim 30$  kHz, amplitude 10 V) was applied to the substrate. This has induced mechanical oscillations of the piezo responsive phase in studied NWs, which was registered by high-frequency lock-in of the SPM controller. In a modified version of piezo experiment, we observed current instead of mechanical oscillations. NWs were stressed, but not broken and piezo potential was induced in them. Therefore, mapping of current flowing through the area with NWs was performed under the gentle force. In such approach, piezoelectric NWs are bended and can generate an observable electric current.

## 2. Electrical measurements

Industrial importance of electrical characterization of NWs defined that electrical measurements of NWs are broadly studied and reported nowadays [7, 53–55]. Indeed, GaAs and InP NWs are proposed for next-generation NW-based solar cells [9, 25, 56–58], while their

efficiency is characterized from current-voltage characteristics of an array of NWs (rarely from single individual NW [11]). SPM electrical measurements can be classified into two main types. First one is registration of electric current and its dependence from voltage applied between contacting probe and sample [7] by C-AFM or PeakForce Tuna methods. Secondly, registration of surface electric potential of a sample (i.e. work function of a NW's surface combined with visualization of injected electrostatic charge), is achievable in lift scan of KPFM.

For proper electrical measurements of NWs, substrate must be highly conductive (**Figure 1a**). Obviously, resistance of a wafer should be significantly smaller than resistance of the NW connected in series with substrate (not more than few Ohms). Therefore, substrates' resistance can be neglected [7, 25] (**Figure 1b**). While probe-NW contact resistance is also neglected and shunting is avoided, the I-V characteristics indicate Schottky barrier near zero voltage [7] and linear resistance of a NW (when Schottky barrier becomes open as will be discussed further in 2.1.1.). Connection to a bias source should be direct and not leading to any significant RLC elaboration. Additionally, SPM probes should be highly conductive with uniform thickness of stable rigid conductive coating. It is important to know the shape of a probe's tip apex and utilize probes with height of the tip pyramid applicable for micrometer-tall NWs. For example, KPFM studies are routinely done by probes with height of a pyramidal tip  $\sim 2.5 \mu\text{m}$ . Such probes must not be used for studies of NWs with heights above  $\sim 2.0 \mu\text{m}$ , because a cantilever's beam would strike NW instead of scanning done appropriately with the tip's apex. Morphology of a sample should be considered from established growth procedure or with subsequent visualization techniques, e.g., SEM or TEM. Moreover, following less articulated phenomena should be kept in mind for accurate measurement.

- "Plowing effect" [59], i.e., sliding of the location of probe-sample contact in opposite direction from the cantilever's holder after probe is approaching onto a sample. Referred contact is arranged between the end of tip's apex and a sample. Sliding between them emerges due to the lateral force acting onto the probe's tip mounted on a cantilever affixed at one end. Such sliding (i.e. plowing) occurs every time when the SPM probe approaches the surface, e.g. during initial engage onto the sample, and in each tapping cycle. Plowing/sliding length can reach tens of nanometers depending on setpoint force and is able to damage the surface of flat soft samples. This phenomenon must be considered to understand where exactly the current-voltage spectrum is being registered.
- Influence of setpoint force of push by SPM probe onto stability of contact and forcing, i.e., penetrating, through a surface oxide and chemisorbed water layers.
- Flexibility of a cantilever with related possibility that both vertical and torsional bends will be represented under dissimilar setpoint forces.
- Geometry of a contact between the round top part of an NW (**Figure 1c**) and rounded SPM probe's tip elongated into a pyramid.

Aforementioned features should be taken into account with environmental conditions of specific experiment, i.e., pressure of ambient gas or vacuum level, composition and humidity of this surrounding medium, temperature of the system, and illumination of certain individual NW under the study. Consideration of these factors is important because environment, e.g. air

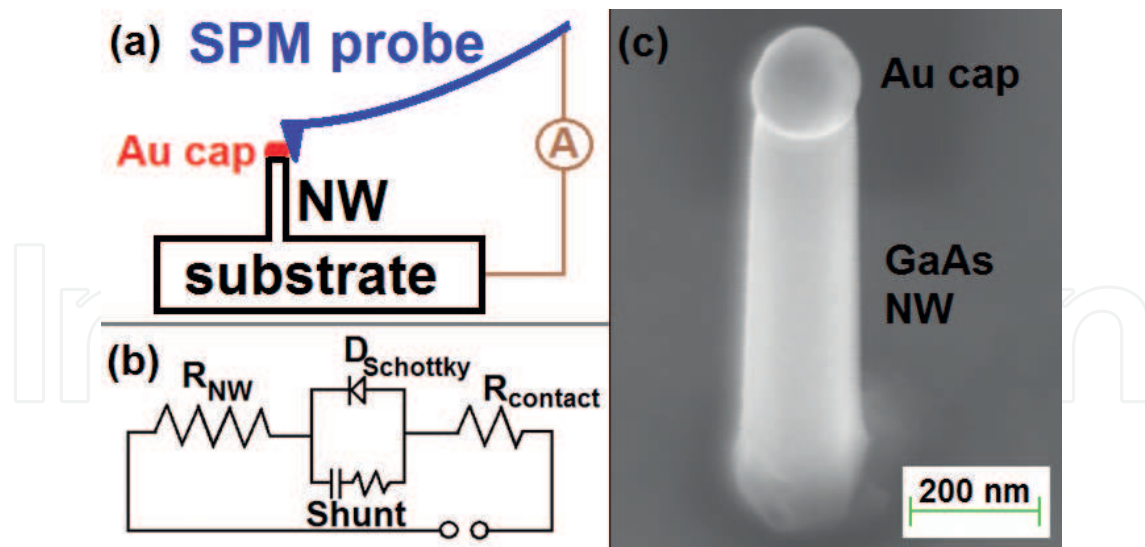


**Figure 1.** (a) Scheme of the electroconductive experiment by SPM probe in contact with an NW's metal cap. (b) Equivalent electric circuit proposed for the electrical conductivity of a semiconductor NW with a metal cap. (c) Single vertical p<sup>+</sup>-GaAs NW on p<sup>+</sup>-GaAs substrate.

in an AFM laboratory room, leads to surface oxidation and covering of NWs by a layer of water. Therefore, electrical, mechanical, and other properties of NWs experience aging. In practice, aging in GaAs is more intensive than for InP, but deterioration of NW can be decelerated by passivation with AlGaAs, GaN, GaP, or other thin coatings [56, 60].

## 2.1. Electrical conductivity of vertical and horizontal nanowires

Electrical resistance of the conductive channel [7, 56] in a semiconductor NW can be measured when bias is arranged between SPM's probe and a NW positioned in direct contact. Later evaluation of transconductance can be done in terms of the thermionic emission theory [7]. It should be noted that high amount of surface states are one of the most widely known disadvantages of GaAs as a material [55]. Indeed, charges can be trapped by NW's surface due to the defective nature of surface of nanostructures. These trapped carriers induce electric charge that hampers transport of mobile carriers through the conduction channel. Moreover, layer of a nonstoichiometric oxide grows on bulk semiconductor material of the NW. This oxide layer similarly acts as a charge-trapping agent blocking the carrier's transport in the NW, i.e., decreasing width of the conductive channel [61].

SPM controller allows measuring small current flowing through the system when contact is arranged with single individual NW. It should be noted that since SPM controller is solely measuring the electric current signal, an adequate model should be used to interpret the obtained signal (**Figure 1b**). Reason is that shunt or parasitic conductance through undesired coatings, e.g. chemisorbed water layer (from moisture content), nonstoichiometric oxide, or passivation layer can influence the obtained I-V characteristics. Capability to measure the as-grown vertical NWs is the main advantage of SPM techniques in comparison to methods requiring breakage and postgrown processing, which affect properties of these nanostructures. Additionally, SPM is preferential to massive methods, where parameters are registered for an

array containing hundreds to millions of NWs, and further experimental values are averaged. Indeed, massive approaches do not allow qualifying the growth quality of NWs and examination of their local features, e.g., properties of Schottky barrier located between metal cap and a semiconductor NW. Thus, the prominent advantage of SPM in research of NWs is exactly in studying of local properties of individual structures.

### 2.1.1. Obtaining the current-voltage characteristics

Approach of taking I–V curves initiates from scanning the area covered by NWs (**Figure 2a**), while DC bias  $\sim 1$  V is applied between SPM probe and a substrate. In modern microscopes, it is possible to record few channels of data simultaneously during a single scan. This provides obtaining of maps demarcating independent records of properties of a studied material when SPM data scan file is analyzed. Later, it becomes possible to correlate features from different channels, e.g., *topography* and *current*, and understand details of certain features observed in overall morphology. Vertical NW appears as pyramids in *topography* (**Figure 2b**) due to convolution effect of pyramidal tip and cylindrical or hexagonal NW. Preliminary map of currents in close proximity to a conductive NW typically represents an ensemble of conductive points or distinctive regions with regular shape indicating currents responsible for different facets of the SPM probe tip's pyramid (**Figure 2b** and **c**).

C-AFM study is considerably less expensive and more automated than similar studies performed on SEM with full metal probe or practice of STM with visualization of movements by the station's SEM [62–64]. Noteworthy that in C-AFM, it is only necessary to choose the location where current is maximum and to perform spectroscopy of current at this specified spot (**Figure 3**). Typically, position of the spot is situated at a distance approximately tens of nanometers from the top part of a vertical NW's metal cap visible from *topography* (**Figure 2b**). Reason here is that the most conductive area only indicates position where contact resistance  $R_{\text{CONTACT}}$  between probe and NW is the smallest.

Capability to observe conductance of long vertical NWs (**Figure 2b** and **3**) highlights benefits of C-AFM technique in comparison to measurements of those done on horizontal NWs connected by lithography. Advantages include simplicity of procedure, availability of standard conductive probes, and absence of necessity in costly additional visualizing SEM. Moreover, utilization of such SEM is associated with bombardment of the nanostructures with focused high-energy electron beam. It can affect conductivity of NWs both when beam is switched on and off. When SEM is performing visualization, the amount of charge carriers within the certain observed NW increases by injection of electrons in SEM observation procedure. Moreover, if SEM beam is switched off, localized charges can persist in surface oxide and spoil the entire sample and measurement. On the contrary, C-AFM is based on standard AFM. A flexible cantilever with highly responsive piezo scanner and bias control system is used in this regime. These features allow measuring morphology and conductivity of fragile nanoobjects with heights more than  $5 \mu\text{m}$  without their breakage. It is possible to arrange experiments with electric bias applied by SPM, although unfortunately, the aforementioned deterioration of NWs by localized charges can still exist.

Nevertheless, few shortcomings arise in SPM method of I–V spectroscopy. As we have noticed from experimental work, drift of the sample occurs during the scanning, so that the spot of measurements moves toward hardly predictable location. It leads to decline of reproducibility

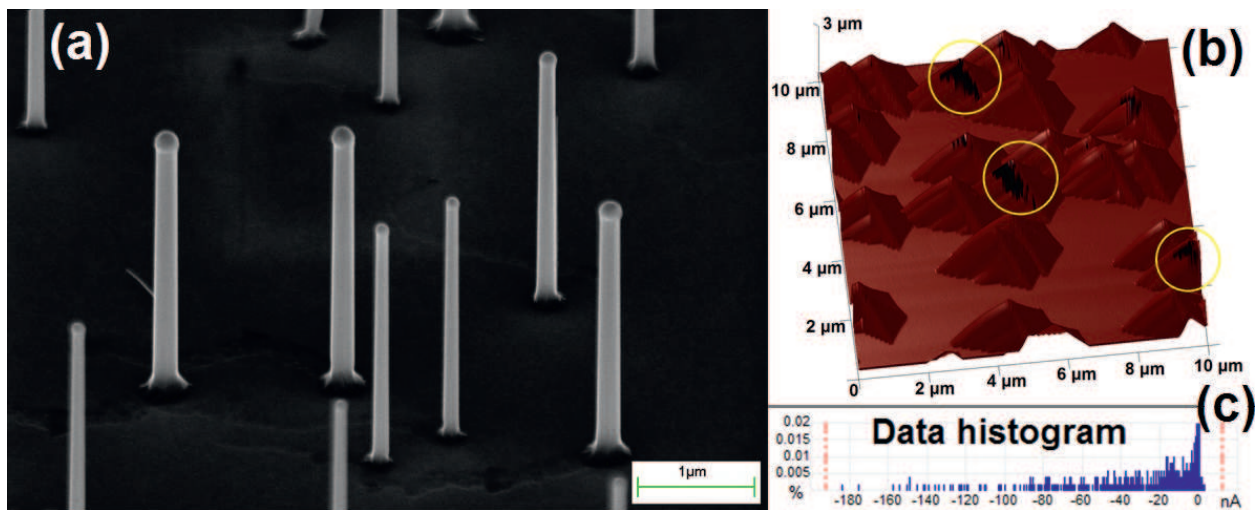


**Figure 2.** (a) SEM image of an array of vertical GaAs NWs. (b) 3D model of topography of an array of vertical GaAs NWs, where NWs are seen as pyramids due to shape convolution. Electric current map is overlaid on 3D topography indicating regions with high current density near the NW tops as black spots marked with circles. (c) Distribution of values of electric currents in an array of NWs obtained by PeakForce Tuna module, where highest absolute values indicate stable electric contact.

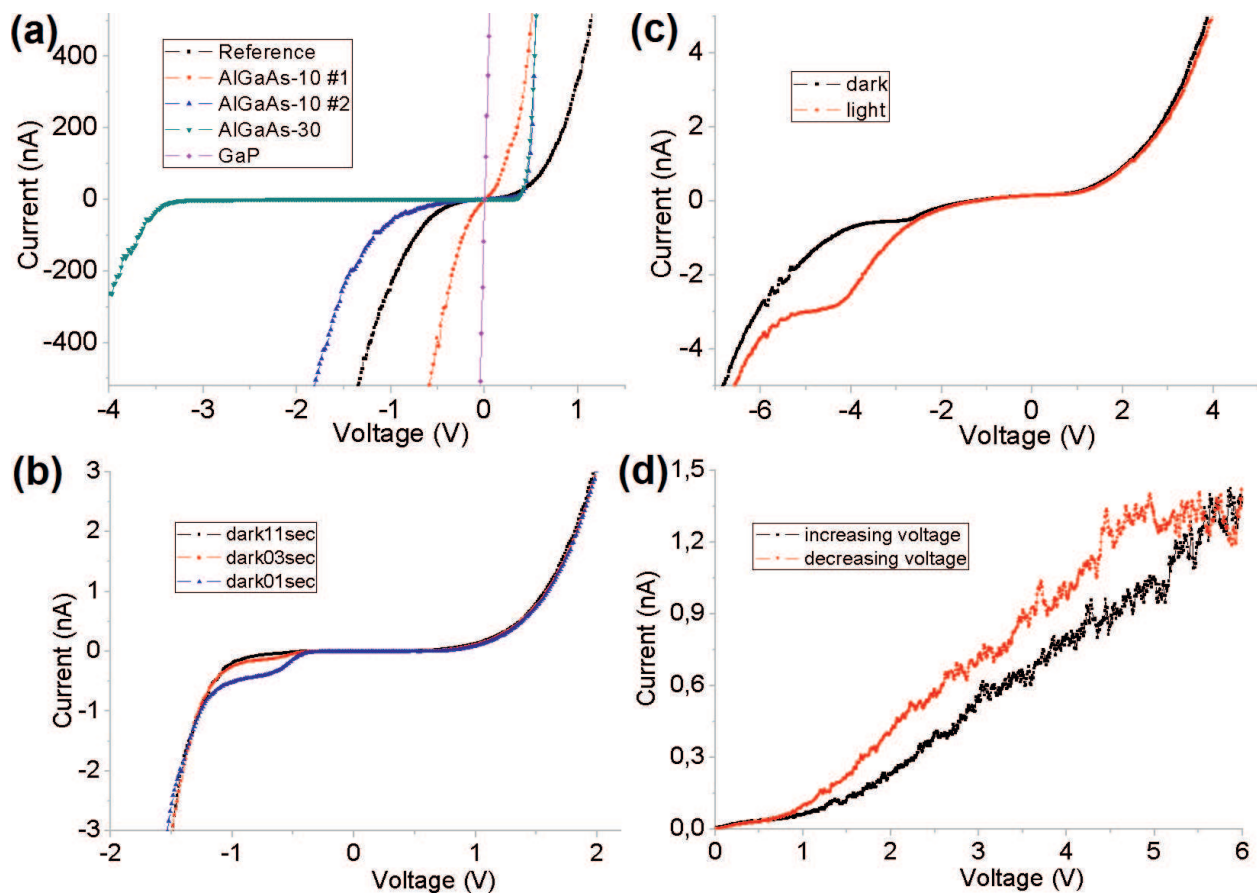


**Figure 3.** I–V curves for vertical (a)–(c) and horizontal (d) GaAs NWs taken by SPM. (a) Comparison of different passivating shells. (b) Indication of effects of sweeping duration onto accumulation of charges in NWs for 1 s, 3 s, and 11 s. (c) Comparison between electric output of the same pGaAs NW on nGaAs substrate in light and dark conditions. (d) Hysteresis of electric current for GaAs NW.

of I–V curves for same NW after long series of measurements. This can be solved by obtaining more representative statistics of measurements, repeating the tests by fresh probes and with significant suppression of a setpoint force acting during I–V spectroscopy acquisition.

Analysis of the I–V spectra [7] (**Figure 3**) acquired by SPM controller for certain individual NWs in a series of samples prepared with different treatments can be done. It is possible to evaluate effects of passivating shell onto conductive behavior of NWs. For example, in **Figure 3a**, two passivating compounds are compared for vertical GaAs NWs, i.e., GaP and AlGaAs. It is noticeable that current through the NW in region of forward bias increases for both of them in comparison with unpassivated reference NWs. We studied these passivating shells in details previously [65, 66]. GaP appeared to be the most advantageous passivating material from experimental measurements of GaAs NWs. This conclusion is obvious from I–V curves taken on vertical NWs since I–V spectra for sample with GaP ultrathin shell demonstrate neither a specific knee in region of forward bias nor the junction voltage parameter. Reason for that is decrease of concentration of surface states at the surface of vertical NWs, which widens the conduction channel in NWs. Practically, I–V curves for GaP passivated NWs were almost linear, so that quasi-Ohmic contact was formed between Au cap and highly doped GaAs crystal part of the NW.

Indeed, latter contact area should arrange a Schottky junction, and NW system should resemble the rectifying shape of I–V curve for a Schottky diode [7, 67] in accordance with the diode law

$$I = I_0(e^{\frac{qV}{kT}} - 1) \quad (1)$$

where  $I_0$  is a reverse-bias leakage current (A),  $q$  is an elementary charge  $1.6 \times 10^{-19}$  C,  $k$  is the Boltzmann constant  $1.23 \times 10^{-23}$  J/K, and  $T$  is an absolute temperature (K).

It is considered that explanation for phenomenon of negligence of Schottky input is that Fermi-level pinning is reduced in highly doped NW [68]. In fact, level of doping can be quantified from the linear serial resistance region of I–V curves. The slope equals to resistance of a system by Ohm's law and following equation

$$R = \frac{l}{eN_A\mu\pi r_{NW}^2} \quad (2)$$

where length of the NW,  $l$ , is approximately 1  $\mu\text{m}$ , elementary charge  $q = 1.6 \times 10^{-19}$  C, mobility of carriers  $\mu = 400$   $\text{cm}^2/\text{V s}$ , and NW's radius  $r_{NW}$  is approximately 50 nm, while carrier concentration is  $N_A$ . Since resistance of GaP-passivated p-GaAs NWs is  $\sim 100$  k $\Omega$  from the slope, the doping level  $N_A$  is approximately  $10^{19}$   $\text{cm}^{-3}$ , verifying the value anticipated from fabrication protocol of VLS growth.

Passivation by GaP [69] or AlGaAs [70] was previously found among the most advantageous methods to decrease the density of surface states in GaAs NWs by other authors. Interestingly, it is possible to distinguish instabilities of quality of passivation for NWs over the single sample as visible for two I–V curves taken on two separate GaAs NWs with equal 10-nm AlGaAs-passivating shells. In fact, sizes of NWs have specific distribution as can be seen

in **Figure 2a**. From AlGaAs passivation results obtained for NW#1 (red curve) and NW#2 (blue curve), it is possible to conclude that thin AlGaAs passivation is also advantageous for GaAs NWs, although effect of passivation is less pronounced comparing with NWs shelled by GaP. However, summarized effect of the surface states (fast traps and slow traps) of native oxide significantly depends on NW's diameter. I–V curve for NW with AlGaAs shell passivation layer with thickness 30 nm (cyan curve) already resembles the shape characteristic for a diode.

Such NWs have forward threshold voltage (junction voltage) approximately 0.2 V and indicate leakage current and reverse breakdown voltage lower than  $-3$  V. Therefore, such thick shell passivation approach is detrimental for NWs. Reason for that is accumulation of electric charge at the shell and its capacitive adverse input blocking the conduction channel of the NW. Moreover, inclination of all curves in regions of linear resistance is equal because it represents the concentration of charge carriers, i.e., same doping level [65, 66].

Furthermore, analysis of curves recorded with different sweeping rates indicates that charge accumulation and redistribution effects can be visualized for GaP-passivated pGaAs NWs on nGaAs substrates (**Figure 3b**). Corresponding curves represent both Schottky barrier input and p–n junction barrier. It should be noted that detailed shape of I–V curves depends not only on sweeping rate (duration of registration of a spectra) but also on starting voltage of such registration and cycle. Latter means that hysteresis effects can be observed from I–V curves of NWs. Therefore, all curves in **Figure 3a–c** were shown for sweeping from maximum voltage, i.e. while bias was consistently shifted toward negative potential. Additionally, illumination effects can be observed for certain NW systems with p-n barrier. As it is seen from **Figure 3c** for unpassivated pGaAs NW on nGaAs substrate, over-lighted conditions led to intensive rise in current through NW. In addition, the serial linear resistance regions for unpassivated NW (**Figure 3c**) are significantly further from 0 V comparing with passivated NWs (**Figure 3b**). Partly, the observed increase of current can be explained by the stimulation of photo-induced conductivity. Availability to register I–V curves is more impressive for vertical NWs but can be done also for horizontal NWs. In this respect, for example, resistivity and charge accumulation near the Schottky barrier (near the interface between the NW and each electrode) can be (**Figure 3d**).

### 2.1.2. Mapping of electric current (C-AFM in contact mode, PeakForce

TUNA in semicontact mode)

Another option is performing the C-AFM scanning without further spectroscopy, while DC bias between probe and sample is being manually or programmably changed. This possesses registering the map of values of current for each manually specified bias. The approach is time-consuming, but can allow plotting of considerable amount of data points on I–V plot and later reconstruction of detailed shape of I–V curves. Advantage of the mapping approach is elimination of the adverse drift, because it is possible to reconstruct the location of a NW's cap independently in every scan. This location of maximum current would be defined to consider and plot exactly current values from the locations of maximum currents. It should be noted that high-aspect ratio, i.e., so-called lent-shaped scans are proposed to be done. These rectangular shape scans with low amount of scan lines along the slow scan axis reduce duration of

SPM measurements. Another advantage is that mapping approach allows obtaining statistics to characterize the distribution and repeatability of conductance of NWs in an array. Unfortunately, mapping approach accelerates degradation of the SPM probe by wearing its conductive coating and can result into damage or breakage of the NW. This is due to significant forces (in the order of hundreds to thousands of nanonewtons) acting onto NWs in contact mode of C-AFM. Stability of conductive coating of SPM probes from wearing can be verified as unflinching of maximum values of registered electric current with time during a series of scans.

Therefore, the most advantageous procedure of measurements of NW's resistance should be based on method, where force of interaction is minimized and controlled. Most of recent SPM setups provide this opportunity, which appeared initially as PeakForce™ mode (Bruker). PeakForce is based on ScanAsyst feature allowing automated calculation of optimal setpoint force and feedback gain. Here, it should be noted that the regime combining both accurate measurement of topography and measurement of current is called PeakForce TUNA mode. The regime is realized as additional mode of our standard SPM microscope. It is beneficial in comparison to C-AFM because considerably smaller force of interaction can be established and controlled, i.e., force is controlled with precision  $\sim 0.01$  nN instead of few nN in C-AFM. Simultaneously, current is being registered in the range up to 500 nA with outstanding accuracy  $\sim 65$  fA, which is also two order of magnitude more accurate than C-AFM with its high noise level. Practically, measurements of morphology of vertical NWs are done in such a way that force of interaction onto flexible few micrometer-tall NWs can be controlled to be approximately 0.1 nN.

Since PeakForce Tuna is a semicontact regime, electric current is being measured in every act of tapping. Direct contact established during a single tap lasts approximately tens of microseconds (depending on setpoint force and tapping frequency), but this duration is enough for modern electronics to register current precisely with picoampere accuracy. This approach allows measurements of long and thin NWs (length  $\sim 4$   $\mu\text{m}$  and diameter  $\sim 10$  nm) without damaging the NWs as was shown in our previous works [65, 66]. Last important detail is exactly the composition of conductive coating on SPM probes utilized for electric measurements. Industrial techniques of fabrication of SPM probes are consistently developing. Old types of coating materials, e.g., so-called diamond-like coated probes (DCP), are becoming more rigid and reliable. Simultaneously, noble metals are being used for coatings, e.g., alloy of Pt/Ir (Bruker) or Au. These coatings have thickness approximately tens of nanometers and tend to be defaced when significant forces or electrical biases above 2 V are applied. It leads to decline in repeatability of results for excessive biases or insufficient scale of applied electric potential for I–V curves. We consider that most reliable results can be obtained with modern DCP probes (NT-MDT), or AFM probes made entirely of highly conductive inert metal, e.g., full metal platinum probes (Rocky mountain nanotechnology) or with SPM probes covered with tungsten semicarbide  $\text{W}_2\text{C}$  (ScanSens). All of these types of probes are available in market representing various resonant frequencies and spring constants. Still unfortunately, progress of SPM probes seems less significant than predicted by corresponding roadmaps for technologies [71]. Hence, a holdback in one of the nanotechnologies decelerates research of others as happens in the study of NWs.

## 2.2. Electrostatic surface potential and charging of horizontal NWs

KPFM is a method of registration of surface electric potential originated from a classical experimental technique invented in late nineteenth century. Its principle of operation utilizes control of electric potential field between measuring probe and studied sample [72]. SPM probe moves in predetermined pattern above the surface with constant lift height and performs mapping of surface's electric potential with millivolt-level accuracy. The advanced SPM version of Kelvin probe setup is KPFM operated in frequency modulation regime. Lateral resolution of imaging is in the order of radius of the SPM tip, while most recent conductive SPM tips have radius approximately 20 nm. Indeed, KPFM can be acclaimed as one of the most important and informative tools to study electrostatic effects in NWs. In a forefront KPFM experimental procedure, scanning is being done in a single pass, simultaneously mapping *topography* and *potential*. This feature is called PeakForce KPFM FM, and it reduces the duration of experiment twice in comparison to two-pass method [73]. Thus, major achievements in this method were reached during latest two decades as a result of advanced nanotechnology and modern computing. It should be noted that resolution of KPFM is strongly dependent on quality factor of SPM's probe oscillations  $Q$ . Parameter  $Q$  increases in vacuum due to depressed damping of induced mechanical vibrations of SPM cantilever that significantly improve signal-to-noise ratio. Common resolution in ambient air conditions is limited by tens of nanometers partly due to the moisture and water layer covering surfaces of both sample and SPM probes.

KPFM experiments with horizontal NWs fixed in metal-semiconductor-metal (MSM) geometry are well established and were described in previous works [74]. However, it seems worth adding few vital previously unreported details to disclose the procedure of surface potential microscopy in even more comprehensive way. Optimal procedure of KPFM measurements assumes that horizontally lying NW (see marked area in **Figure 4a**) should be oriented perpendicularly to the plane of the vertical deflection of an SPM cantilever (see scheme in **Figure 4b**). Typically, this is achieved by manual rotating of the sample itself or sample's holder in desired direction before the measurements. Scanning should be done with fast scanning direction coincident with long axis of an NW, which is done by insertion of scan angle of  $90^\circ$ . These methodical improvements result into elimination of influence of shape of the pyramidal SPM tip because front and back angles of the tip pyramid are typically different, while the two other side angles are identical. Another benefit is a significant suppression of parasitic capacitive influence of massive SPM tip onto lateral resolution [75]. Moreover, such arrangement routinely eliminates spikes related to topography roughness of NWs visible in lift pass of the double pass KPFM mode. This is because typical surface profile of the NW in the direction of fast scanning is a smooth flat line. Latter allows decreasing the lift scan distance below 20 nm without any risk of accidental contacting the NW in a noncontact pass. Cantilever and the pyramidal tip should be as small as allowed by features of topology and roughness. In addition, tip radius need to be as small as possible on probe with stable conductive coating. Consideration of all aforementioned factors can allow sub-nanometer resolution of KPFM imaging [72].

Injection of electric charge with its subsequent registration by SPM involves the following steps. Electric bias should be switched on and adjusted to zero with feedback system recording

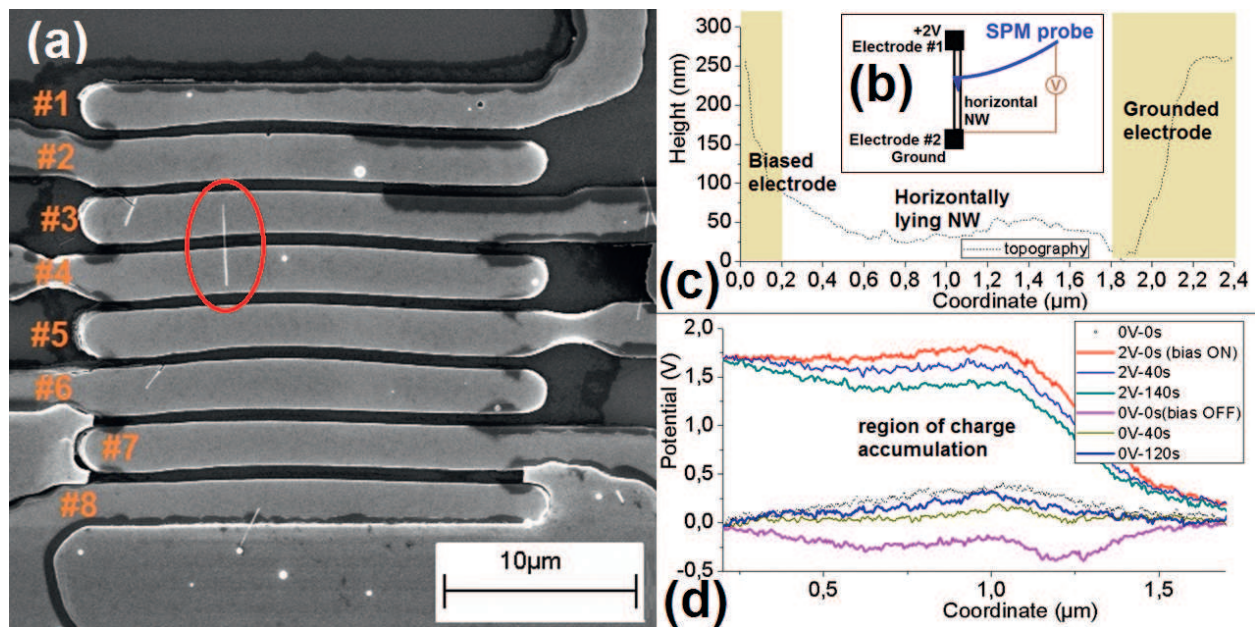


**Figure 4.** (a) SEM image of a microscheme with pGaAs NW covered by Zn-Au micropads grown by optical lithography. Red mark indicates an NW circuiting the pads #3 and #4, which were used for biasing and grounding. (b) Scheme of the surface potential experiment by SPM probe lifted above the horizontally lying NW. NW is rotated on scheme to represent perpendicular direction of its axis to bending plane of the SPM's probe. (c) Topography profile of the horizontal pGaAs NW. (d) Surface electrical profiles for bias 2 V applied followed by 0 V applied to the left electrode, i.e., to electric micropad #3.

electric *potential* of a sample. First, surface *potential* map should clearly indicate position and orientation of an NW on a substrate in *topography* (Figure 4c). It is expected that *potential* profile of the NW should be smooth and flat (Figure 4d). If NW is properly connected to microelectrodes and further massive electric feed source, then *potential* of the electrodes should immediately reflect the established parameter of DC bias (i.e., zero if grounded). It should be highlighted that surface *potential* profile of the NW would follow the set value of electric potential of an electrode. It is remarkable that the profile can change in time due to accumulation of electric charges so that shape of profile evolves depending on barrier and NW (Figure 4d). Moreover, shape of the profile qualifies this energy barrier at the border between two materials, which indicates certain type of electric contact, i.e., Ohmic [65–67] or Schottky (Figure 4d).

Furthermore, potential of both electrodes immediately returns to initial value when bias is switched off, but the distribution of surface electric potential profile of an NW in KPFM occurs with finite observable rate (Figure 4d). It means that exactly the charge injected into the NW is visible in profile. Reason is that accumulated charge whose highest concentration is located at coordinate of maximum  $U_{MAX}(x)$  is distributed according to (1) diffusive transport model, (2) tunneling into substrate, and (3) considering Coulomb repulsion [76]. In other words, electric charges become redistributed and dynamics of this process are restricted by certain major distribution mechanism. The major mechanism of charge distribution in semiconductor NWs should be diffusion. If charge is leaking, then transistors and energy sources produced on base of such NWs would be ineffective. This means that for properly arranged transport

measurements with SPM  $dU(t)$  should be proportional to square root of time. From  $U_{MAX}(t)$  dependence and full-width at half-maximum of  $U_{MAX}(t)$  plot, it becomes possible to characterize the mobility of charge carriers and location of defects in NWs. It should be noted that experiments in horizontal NWs and recording their surface potential profiles are preferable to be done for NWs fixed at two ends in a “bridge geometry” [77, 78]. The “bridge geometry” arrangement is laborious in fabrication, although superior to the horizontal MSM arrangement. Reason is that in bridge geometry, the NW is not in electrical contact with a substrate, which eradicates possibility of charge tunneling into the substrate. Similar KPFM investigation over the length of the NW can be proposed also for vertical or inclined NWs, although the substrate with such NWs must be cleaved and then tilted so that SPM probe would have access to the side surface of the NW instead of solely the NW's metal cap. Potentially, electrical studies of NWs can be done by an SPM probe oriented horizontally [79] but not with vertical standard AFM and STM probe tips. In addition, multiprobe techniques already allow advanced operation with vertical NWs [80], but such measuring stations are nowadays expensive and rare.

### 3. Evaluation of mechanical strength for inclined NWs

Evaluation of strength characteristics of nanoscale objects is a nontrivial task, particularly because it is impeded by properties of their surface, geometry of a measurement, and physical effects of scaling. In this respect, studies of NWs by SPM are challenging because these structures are highly bendable, oscillate with own frequency due to thermal vibrations, and because properties along the NW can be unevenly distributed. Another challenge is that NWs kept in atmospheric environment become partly oxidized, and their properties tend to resemble features of nanocomposites. One of the major details that are widely neglected is that NWs represent specific degree of tapering (**Figures 1c, 2a, and 5a**). Reason for that is parasitical input of vapor-solid input of crystal growth [52], which occurs concurrently with VLS mechanism. Tapering of group III–V semiconductor NWs is more pronounced under high-temperature fabrication and for excessive values for relation of V/III precursor sources inside a MOVPE chamber [50]. We will pay special attention to the impact of tapering onto measurement of properties of NWs in this section.

Few methods possessing nanoscale accuracy enable measurements of 1D nanostructures. One of the noncontact approaches makes use of in-situ TEM in order to measure amplitude of free and induced mechanical oscillations of an NW fixed at one end [81]. To certain degree of accuracy, it is possible to calculate elastic parameters with such TEM or high-resolution SEM visualization. Typically, it is only needed to calculate elastic modulus from abovementioned amplitude and geometrical parameters with known density of the NW's material. However, first, certain degree of inaccuracy arises from inexactness of measured geometry and vibrational output. Second, the major reason for error can be that no adequate models were proposed for tapered structures and their mechanics. It should be noted that flexibility coefficient of such tapered NWs is variable along the length.

Methods based on SPM employ direct mechanical contact between structure and a probe and have advantage in their locality. In fact, the only SPM approach presented in literature is when the

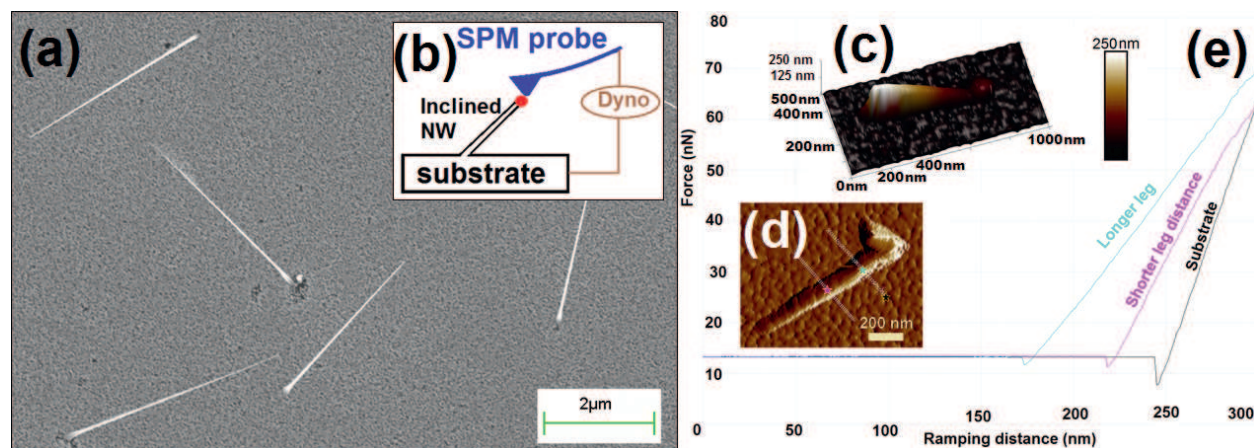


**Figure 5.** (a) SEM image of an array of inclined tapered wurtzite InP NWs on Si substrate. (b) Scheme of the bending experiment by SPM probe brought in contact with inclined NW. (c) 3D topography model of an inclined NW representing angle  $22^\circ$  for visualization of the NW under small setpoint force. (d) PeakForce error channel representing NW's fixed end at lower left and free end at upper right. Force spectroscopy was performed according to the coordinates seen by color marks. (e) force-load curves  $F(z)$  for substrate, middle of NW, and free end of NW.

probe is bending an NW in a definite leg distance point [82, 83]. Leg distance and NW's diameter should be accurately measured in order to evaluate the Young's modulus. We will describe this simple approach in detail at first and then represent our original approach based on mapping of elastic parameters. Latter allows precise control of setpoint force that provides significantly more accurate and precise results for tapered NWs, also entitled as conical NWs or nanocones [84].

### 3.1. Method of force-load curves $F(z)$

The simplest approach is based on bending of an NW by SPM probe in exactly defined position [85]. This experiment can be performed on inclined cylindrical NWs (Figure 5a–c). Procedure involves measurement of *topography* and defining the location, where stable contact for bending can be established at farthest distance from the NW's fixed end (Figure 5d). Longer leg distance provides higher values of displacement and thereof bigger amount of data points plotting the  $F(z)$  curve without breaking the NW.

SPM probe for such experiments needs to be flexible and dull, i.e., tip radius is desirable to be considerably more than 30 nm. Initially, cantilever becomes bended on any flat rigid substrate (see black curve on Figure 5e), e.g., in proximity to the NW. When spring constant of SPM cantilever becomes precisely recognized, the measurement is called calibrated conferring the force-distant curve  $F(z)$  and its slope. Afterward, bending of the desired structure is performed. It is clearly visible that magenta and turquoise curves (Figure 5e) taken correspondingly for location near the middle length of the NW and closer to the free end indicate two different slopes. For a highly bendable structure, measured force-load curve  $F(z)$  will consist of two components, i.e., bending of a cantilever and own bend of the NW [85]. For finest evaluation of the NW's spring constant, it is preferable to choose a cantilever with spring constant similar to the anticipated stiffness of the NW. Since spring constant of cantilever  $k_{\text{CANT}}$  is known from calibration, the other component is exactly spring constant of the NW  $k_{\text{NW}}$  [85].

First difficulty of this one-point spectroscopy approach is that NWs can be tapered to specific extent. Their diameter  $d_{\text{NW}}$  is depending on leg distance  $x$ , but since  $d_{\text{NW}}(x)$  is changing along the length of the NW, then their  $k_{\text{NW}}$  is nonlinearly dependent from leg distance as  $k_{\text{NW}}(x)$ , where  $x \in [0; L]$ . Despite that,  $k_{\text{NW}}$  characterizing elastic properties of a studied NW is adequately obtained only for one coordinate situated considerably far from NW's end. Second, it does not seem achievable to recognize this leg distance  $x$  precisely, because inclined NWs are partly merged with the substrate at the fixed end, which is an artifact of fabrication procedure (**Figure 5d**). However, it is obvious that SPM probe is unable to visualize any area beneath the structure (**Figure 5c**). Third, since diameter strongly affects the value of elastic modulus, inaccuracy of a diameter is crucial. Finally, such measurement can hardly be qualified as stable, because sliding effect is significant, so repeatability over time is also a significant drawback. Nonetheless, with this technique authors of [82, 83, 85] have successfully measured and reported elastic moduli of 1D nanostructures with reasonable accuracy. It was achievable because method of force-load curves is adequate for thick long nanostructures.

### 3.2. Advanced QNM for bendable nanostructures

We have generalized an advanced procedure allowing measurements of inclined NWs to be carried out with significant accuracy [86]. Measurements are proposed to be performed with the help of SPM equipped by a module registering setpoint force at each moment, e.g., QNM. In fact, major SPM manufacturers had promoted concurrent methods analogous to QNM (HybriD from NT-MDT, pulsed force mode from WITec and jumping mode from Nanotec Electronica) independently, while Bruker firstly introduced their QNM™ in 2009. As a result, this advanced experimental technique is now attainable by plenty of research teams with various microscopes worldwide. Let us describe our experimental approach with theoretical background and associated limitations, which will be formulated in terminology of the Bruker's QNM mode.

Initially, it is possible to find individual NWs by built-in optical microscope providing magnification 200x. In fact, even location of thin NWs having diameters 10 nm can be visualized by optical microscope, because they scatter the light. Such NWs become visible as single grey pixel routinely resolvable by optical matrix (**Figure 6a**). The scanning is done by the blunt flexible SPM probe moving along the long axis of an inclined NW. It should be noted that specific probes can have a tip shape allowing to settle on the nanostructure and arrange a stable mechanical contact. For example, manufactured NP-STT10 probes (Bruker) with two tip apexes are proposed for stabilization of contact between NW and SPM probe and to avoid sliding effect (see two tip apexes in **Figure 6b**). Separately, ordinary flexible one-apex probes should be used for surface visualization. QNM measurements of bendable NWs are proposed to be performed under different setpoint forces (**Figure 6c** and **d**) in order to obtain significant statistics to calculate flexibility coefficients (**Figure 6e**) and model the Young's modulus. Interestingly, such remarkably precise scanning requires not more than 10 min with rectangular scans described in Section 2.1.2. Entire profile of a flexibility coefficient is obtained instead of low representative single data point in the method of force-load curves (**Figure 5e**). These data are reproducible during the scan, for different forces and by probes with different spring constants.

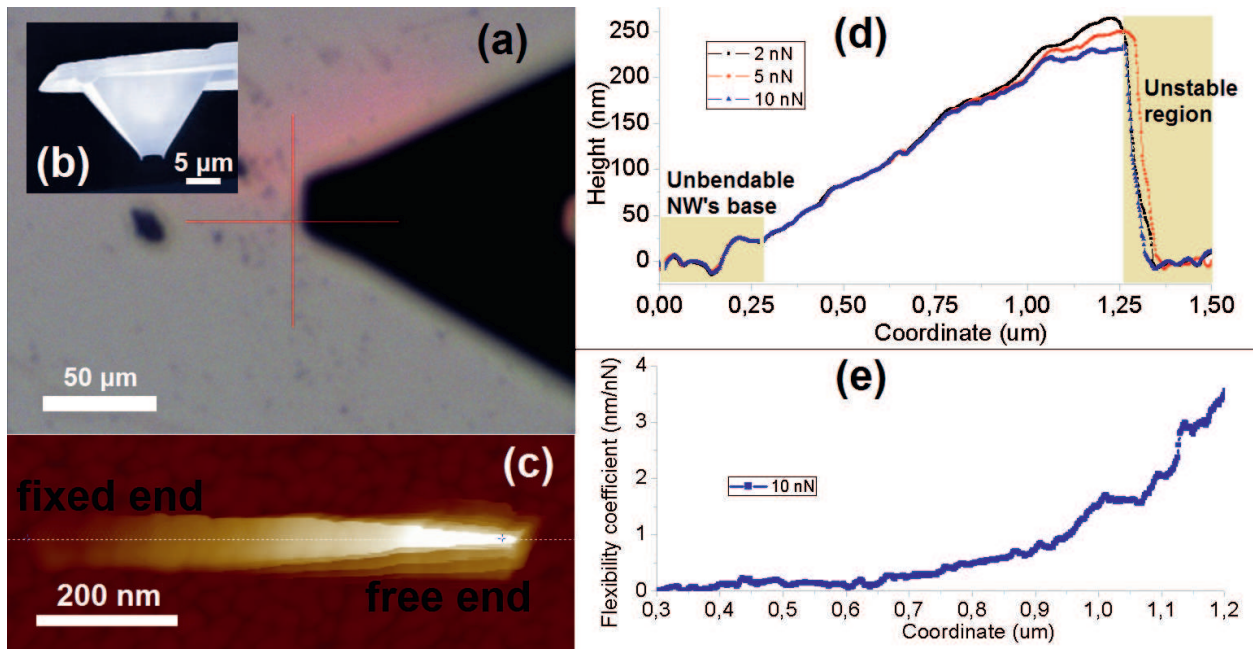


**Figure 6.** (a) Optical image  $125 \times 80 \mu\text{m}$  representing individual NWs as grey spots near the triangle-shaped SPM cantilever. (b) SEM image of BRUKER NP-STT10 probe with two apices at the end of the tip and an arc between them. (c) High resolution rectangular shaped 2D topography image of an inclined InP NW under significant force setpoint 10 nN. (d) Comparison of topography profiles for bending of inclined InP NW under different forces. (e) Bending profile representing flexibility spectra of a single bendable NW along its length, where fixed end is on left and free end is on right side.

Our approach is based on Hooke's law and Euler-Bernoulli theory. The body compression law (seventeenth century Hooke's law) states that

$$F = k\delta \quad (3)$$

where  $k$  is a linear stiffness coefficient, i.e., spring constant, of a structure and  $\delta$  is a linear displacement, i.e., deformation, by the force  $F$  acting on same axis with deformation.

In case of a NW, which is bended down by specific setpoint force  $F$  until the NW's "bended position", the equation for deflection  $\omega$  should be written as follows

$$F = k_{NW}(x) \cdot \omega_{NW, F}(x) \quad (4)$$

Noteworthy that the "spring constant"  $k_{NW}$  is not invariable along the NW structure in bending experiment, but depends from a distance to the fixed end  $x \in [0, L]$ , where  $L$  is length of NW.

Deflection of NW  $\omega_{NW, F}$  under certain applied force  $F$  is a parameter measurable from SPM topography data (**Figure 6d**)

$$\omega_{NW, F}(x) = \Delta\text{height} = h_F(x) - h_0(x) \quad (5)$$

where  $h$  is a registered height, so that  $h_{10\text{nN}}(x)$  is the height observed by SPM when the probe pushes with a setpoint force 10 nN at a certain coordinate  $x \in [0, L]$ .

It should be noted that  $F$  is a fixed parameter and this setpoint force is established with piconewton accuracy in QNM. The spring constant  $k$  is known as dependent from the leg distance  $x$ , so that relation between  $k$  and  $x$  is cubic for a cylindrical beam  $k \sim x^3$  similar to experimental plot of flexibility profile  $f(x)$  in **Figure 6e**. We will later calculate how exactly  $k$  is related with  $x$  for a tapered beam with the cone angle  $2\alpha$  and diameter in the middle of the NW's length  $D_{\text{MID}}$ . Height  $h_0(x)$  is typically considered as the height of a structure scanned by SPM. Despite that, the topography is always measured under specific setpoint force applied by SPM. Therefore, the force for  $h_0(x)$  is neglected. SPM setpoint force is  $\sim 10$  pN for a gentle scanning, which is affordably small.

Euler-Bernoulli theory introduced in eighteenth century defines bending of an isotropic beam [87], depending on composition (by elastic modulus) and geometrical shape of a beam (e.g., by length  $L$  and diameter  $D$ )

$$\frac{d^2}{dx^2} \left( EI \frac{d^2 \omega}{dx^2} \right) = q \quad (6)$$

where  $I(x)$  is second moment of inertia of a beam.

The equation for deflection of an NW by a point contact established by an SPM probe along the location in NW  $x \in [0, L]$

$$E \frac{d^2}{dx^2} \left( I(x) \frac{d^2 \omega}{dx^2} \right) = 0 \quad (7)$$

The boundary conditions appropriate for our model are

$$\omega(0) = 0; \omega'(0) = 0; \omega''(L) = 0; \omega'''(L) = -\frac{F}{EI(x)} \quad (8)$$

Accounting these boundary conditions, the generalized form of a solution of Eq. (7) is

$$\omega_{\text{NW},F}(x) = \frac{F}{6EI(x)} (3Lx^2 - x^3) \quad (9)$$

The second moment of inertia for a cross-section of a conical beam is described as

$$I(x) = \frac{\pi D_{\text{MID}}^4}{64} \left( 1 + \frac{\alpha}{D_{\text{MID}}} (2x - L) \right) \quad (10)$$

We now can formulate the dependence of flexibility of a tapered NW:

$$f_{\text{NW}}(x) = \frac{1}{k_{\text{NW}}(x)} = \frac{\text{Deflection}}{\text{Force}} = \frac{\omega_{\text{NW},F}(x)}{F} = \frac{1}{E_{\text{mat}}} \cdot [\text{coeff}(x, L, D_{\text{MID}}, \alpha)] \quad (11)$$

where flexibility coefficient  $f_{\text{NW}}(x)$  is presented as a function of material ( $E$ ), location of applied force ( $x$ ), and the shape of a structure ( $L, D_{\text{MID}}, \alpha$ ).

Finally, the formula for calculation of the Young's modulus of a tapered NW in our model is the following

$$E_{\text{mat}} = \frac{64}{3\pi} \frac{1}{f_{\text{NW}}(x)} \frac{1}{D_{\text{mid}}^4} x^3 \frac{1}{\left(1 + \frac{\alpha}{D_{\text{mid}}} (2x - L)\right) \left(1 - \frac{\alpha L}{D_{\text{mid}}}\right)^3} \quad (12)$$

It must be noted that for appropriate application of any model, it is vital to consider not only the generalized form of relation between variables, but also assumptions of the model, defining its limits of use. Two of such assumptions for Euler-Bernoulli theory are isotropy of the material and elastic regime of bending. Material of the NW is considered isotropic across its entire length, discarding e.g., surface effects, possible defects in crystal structure, etc. In reality, defects act as deformation accelerators and result into spikes visible on bending profile. Elastic regime of bending means that object's deformation should be very small with the force applied. In addition, elastic modulus in our model is considered independent from temperature and speed of bending. In fact, Young's modulus  $E$  descends with heating [88], although it is not considered in our model. Indeed, any physical body becomes heated when the work is applied upon it. Therefore, bending by SPM probe performed in a regular manner 2000 times per second can be seen to add heat into the studied NW. Reason for ignoring the possible thermal input is that NWs have considerably high thermal conductivity and small length, so that heat is rapidly distributed into the substrate and dissipated in atmosphere.

Remarkably, the value of Young's modulus is obtained for one-single NW from a substantial series of data points  $\omega_{\text{NW,F}}(x)$  recorded by SPM. Indeed, each of these values is already appropriate to define  $E$ , but the series of data values contains  $\sim 400$  informative data records providing high reproducibility of a result. Furthermore, each setpoint force provides specific bending to verify that deflection is within the linearity range. If multiplied by amount of data values for each applied setpoint force, then significant approximation of flexibility coefficient is achieved, providing unprecedented accuracy of this approach.

Unfortunately, the model involves few geometrical parameters of NWs, which are difficult for estimation with significant accuracy. Visualization techniques, e.g., SEM or SPM topography measurement, were used to provide  $L$ ,  $D_{\text{MID}}$ , and  $\alpha$ . Due to limitations of lateral resolution of SEM scanning ( $\sim 2$  nm) inaccuracy of measurement of diameters of the studied NWs was significant. Moreover, relative error of diameter evaluation increases for thin NWs, while we have studied NWs with diameter of top part as small as 10 nm. Therefore, a special protocol of estimation of diameter of the NWs was utilized to correct the values. Initially, sizes were controlled during fabrication with accuracy approximately  $\pm 3$  nm. After the fabrication, diameters were controlled by SEM. After that we performed breakage of few NWs from an array to estimate their height, while NWs were lying on flat substrate. As a result, for NWs with  $D_{\text{MID}} = 40$  nm, relative error of estimation of Young's modulus was  $\pm 40\%$ . Therefore, we performed the HR-SEM investigation and numerical modeling that decreases the relative error until approximately 20%.

This level of accuracy allowed defining that the Young's modulus of InP in thinner NWs increased from  $60 \pm 7$  GPa until  $140 \pm 30$  GPa. Remarkably, 62 GPa is exactly the value of Young's modulus of zinc blende InP. The result was obtained from a series of 16 inclined

NWs. This means that Young's modulus of wurtzite InP is approximately twice bigger than that of zinc blende InP. Wurtzite structure of NWs was verified by TEM and microPL analysis. Already this, i.e., estimation of Young's moduli of wurtzite InP, is a challenging achievement, which can be acquired only in thin NWs. Reason is that wurtzite InP phase is unstable with increasing of the sample's size, so that bulk material transforms into zinc blende structure while the NWs under our studies were affordably thin. Own scaling effects of Young's modulus of wurtzite phase can be separately investigated when size of the material becomes lower than 50 nm in diameter. Another issue to highlight is that a proper model of tapered NWs was proposed and used [86], which was not performed by other authors. The results were achieved for NWs with upper diameter (width of Au caps)  $\sim 10$  nm.

In order to understand the unlikeness of experiment with bendable objects, it is essentially important to differentiate between "stiffness of the structure" and "rigidity of the material within a structure". Such distinguishing seems necessary because *deformation* channel data are calculated only in the case when both force applied and material's stress occur at the same location. These calculations for SPM in QNM are done in accordance with Derjaguin-Muller-Toporov (DMT) elastic model [24], used as built-in in QNM mode. Indeed, DMT model was introduced in SPM to be mainly used for characterization of flat surfaces and the method succeeded in this pursue. However, for bendable objects, DMT channel data and underlying model are inapplicable. This is explained considering that the stress occurs solely at the fixed end of a bendable structure possessing one fixed end. Therefore, the location of stress (fixed end) is situated micrometers away from location of force applied by SPM probe. In QNM, while DMT model is used, the deformation is quantified from adhesion data, while setpoint force is precisely controlled by feedback system. Topography is being registered routinely, but highly bendable NWs are twisting down during their scanning. Thus, bending reflects on registered topography. Similar conclusion that morphology depends on setpoint force applied by SPM probe was previously demonstrated in studies of exceedingly soft materials [89]. Force needs to be kept in such small range that deformation is consistently  $\sim 1$  nm across the entire flat surface of a sample. Lastly, topography must be measured in appropriate time moment of PeakForce procedure. The sync distance parameter needs to be manually adjusted to be approximately 6  $\mu$ s (for PeakForce frequency 2 kHz) later [86] than established automatically during the first engaging onto a sample prior to scanning. Autofitting of time moment of the PeakForce value for each tapping cycle can solve this problem and probably will be introduced in forthcoming versions of SPM software.

Considering other types of experiments possible to be realized with SPM, classical indentation can be mentioned. For indentation measurements, sharp and extremely stiff SPM probes are required. Unfortunately, elastic deformation and indentation models consider different geometries and types of stress and should not be compared. Elastic models include stretching, squeezing, and torsional stress, while indentation results depend on a shape of the indenter, etc. Interesting summary of results obtained by these various methods of ZnO NWs was prepared by authors of [90]. They have shown that elastic modulus of ZnO measured by different groups with different methods varied by almost twice.

Summarizing that the above-described elastic profile mapping approach is significantly more advanced in comparison with spectroscopic method of investigation of Force-Load

curves. It is first because diameter  $D$  is not considered constant due to tapering of NWs. Secondly, because  $k_{\text{NW}}(L)$  is being evaluated at plenty of definitely established positions, but not at one single location (typically at the oscillating free end of NW and in disfavoring semicontact tapping mode). Our approach allows precise definition of coordinates of the fixed end necessary for the evaluation of the leg distance for each definite data point from hundreds of those measured experimentally. Even though defining these coordinates is not possible for SPM visualization, it is reachable for fitting procedure in our numerical model. Accuracy of evaluation of Young's modulus seems to be approximately 5 GPa for NWs with radius above 30 nm. Finally, our approach is easily applicable for conical NWs. The presented comparatively easy SPM procedure of measurements of elastic characteristics is proposed to be used for various one-dimensional nanostructures and conical nanoobjects.

## 4. Studying piezo response

Piezoelectricity in NWs is an electromechanical phenomenon [91], so we left it to last section of this chapter. Piezophototronic devices based on NWs are widely discussed as sources that would replace both solar cells and windmills in the distant future. Therefore, such nanogenerators based on piezo responsive NWs represent a new generation of sustainable energy sources and must be studied in details. Interestingly, SPM is exactly the instrument that is used by plethora of research teams in the field of nanogenerators of electricity. Previously, we reflected two types of experiments, i.e., spectroscopy and mapping. Being consistent with this methodological assemblage, two self-determined PFM approaches will be discussed in this section for wurtzite GaAs NWs (**Figure 7a** and **b**). First type is a standard PFM oriented toward detection of reverse piezo coefficient. Second type is registration of piezo current and indirect evaluation of piezo coefficient, although reasons for generation of current in this case are not entirely understood up to recent moment.

### 4.1. Reverse piezo coefficient studies of horizontal NWs and nanowire stumps

Experiment requires reliable contact to be arranged between a sample and a dull probe mounted on a stiff cantilever. This is one of the methodical differences comparing to all other experiments described in this chapter where flexible levers were much preferable. Hard contact commonly leads to destruction of vertical and inclined NWs due to significant forces applied to the sample and fragility of NWs. Thus, the method is applicable either for horizontal NWs or for "stumps" (**Figure 7b** insets (i) and (iii), correspondingly). Stump structure is a residue of NW left after its upper part was broken due to application of excessive force (nonelastic stress). The part left is lower than initial NW, so its thermal oscillations are less intensive in lateral direction. Unfortunately, it seems impossible to predict existence of piezo responsive phase in the stump after the breakage. Nevertheless, this becomes explicit from PFM imaging, where studies are performed in C-AFM contact regime.

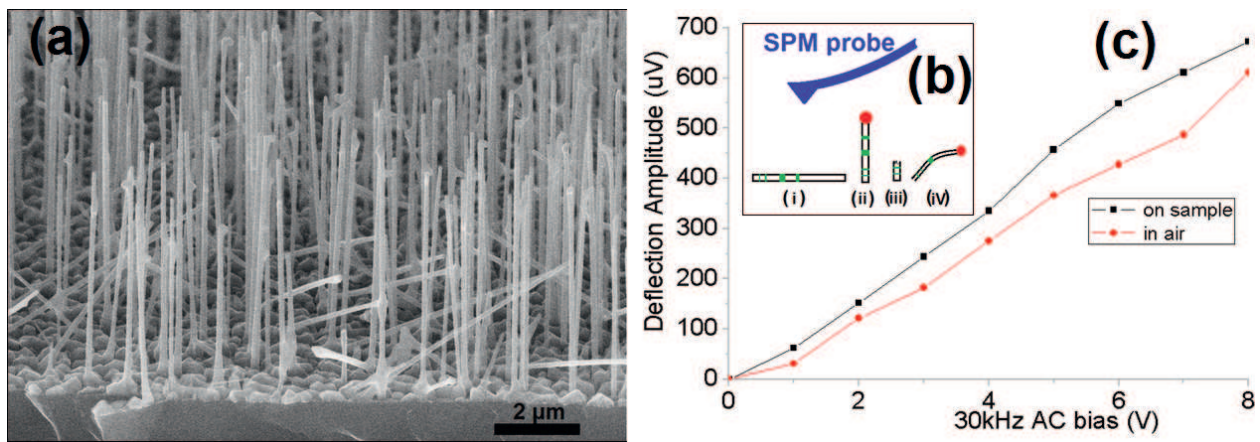


**Figure 7.** (a) SEM image of an array of vertical wurtzite GaAs NWs grown by MBE on Si substrate. (b) Schemes of the PFM experiment by SPM probe for horizontal (i), vertical (ii) and inclined (iv) NWs and NW stump (iii). (c) Comparison between PFM amplitude output from a stump of wurtzite GaAs NW and air 5 μm above the NW.

#### 4.1.1. Spectroscopy of surface oscillations in comparison with non-piezoelectric phase and air

In spectroscopic PFM method (**Figure 7c**), it is necessary to establish a point-like contact (area of contact is few tens of square nanometers) with NW's segment containing piezo responsive phase. Then, high-frequency variable bias  $V_{AC}$  is being applied to the substrate. Frequency of the voltage applied  $f_{AC}$  should be different from the resonant frequency of the SPM probe contacting sample under certain force. After that, mechanical oscillations [ $\mu V_{DER}/V_{AC}$ ] are registered by high-frequency feedback amplifier of photodetector's signal. Indeed, all signals obtained in SPM are processed as relation of *derivative microvolts*  $\mu V_{DER}$  of signal, but if measurement is properly calibrated considering sensitivity of photodetector as [ $\mu V_{DER}/nm$ ], then result would be represented in [ $nm/V_{AC}$ ]. In addition, flexibility of the SPM cantilever can be easily calibrated in [ $nN/nm$ ] (see probe calibration protocol in Section 3.1), which would provide a value of inverse piezo coefficient of a studied material in [ $nN/V_{AC}$ ]. Unfortunately, given force in [ $nN$ ] does not represent the value of elastic response correctly in contact mode AFM, but is used only as guiding parameter of force. However, if standard test sample with known piezo coefficient is used for comparison of its piezo response with data recorded for unknown material, then result for sample would be recorded in standard layout [ $nN/V_{AC}$ ]. In such a way, it becomes possible to compare properties of new materials with references and tabulated data for  $d_{33}$  vertical piezo coefficient for stumps or  $d_{13}$  and  $d_{15}$  coefficients for horizontal NWs.

It should be noted that measurements of both piezo active phase and nonpiezo active phase in same conditions should be compared to eliminate the influence of background noise onto derived signal and evaluate solely input of piezo response (**Figure 7c**). This is due to capacitive effects influencing the compelled resonant mechanical oscillations of an SPM probe situated in micrometer distance from the sample. Obtained dependence of mechanical oscillations from applied potential can be wrongly interpreted as pure piezoresponse signal (**Figure 7c**). The logic here should be that if signal in certain NW is different from measurements of nonpiezoelectric material with same geometry and composition, then piezo phase exists in the NW. Fortunately, single experimental measurement requires few minutes, which permits quick

finding the NW stumps with piezo phase. Significant drawback of this approach is that it is almost impossible to characterize thickness of the piezo active inclusion in the stump, while all remaining part of NW cannot consist of piezo active material. Therefore, additional tools are required to characterize its structure and composition.

#### 4.1.2. Mapping of mechanical oscillations induced by AC voltage

Method of mapping allows avoiding the sample's drift and builds up a map of piezo response (**Figure 8**). Such map indicates more intensive contrast for areas with stronger piezo signal.

If a sample is homogeneous or provides areas with homogeneous piezo response, e.g., on surface of horizontal NWs, then such areas provide significantly representative array of data. Thus, measurements in PFM mapping approach are more accurate comparing with PFM spectroscopy. Drawbacks of this approach are that sample and probe are more intensively worn and torsional movements are strengthened due to friction. Moreover, triboelectric effect arising from friction between SPM probe and surface can influence the result [92]. Triboelectric effect can generate localized charges of opposite signs in the NW and SPM probe after each tap due to friction and difference in work functions between the sample and the probe. These charges can shift surface potential of a sample and lead to generation of adverse current. However, such current is detrimental solely for evaluation of piezo coefficient. Intriguing new field of NW technology was formulated during last decade focused on production of current with triboelectric effect. For comprehensive analysis of prospects of triboelectric nanogenerators, reader should access [92].

## 4.2. Piezo current visualization for vertical and inclined NWs

Instead of reverse piezo effect, it can be more beneficial for applied science and industry to evaluate useful electric current produced by NWs containing piezo responsive phase. We will briefly describe its phenomenological value. Visualization of electric current for thick, vertical, and inclined NWs (see insets (ii) and (iv) in **Figure 7b**, correspondingly) is considered uncomplicated for SPM with force control (see Section 3.2). Latter can be crucial for testing of NWs fabricated from new materials with the following two techniques.

#### 4.2.1. Recording of current during mechanical bending in local point contact geometry

In the method of force-load curves (discussed in Section 3.1), it is possible to perform spectroscopy of current in time  $I(t)$ . If registration of current flowing through the system is switched on, then it becomes possible to measure electric current flowing through an individual NW in every moment of its bending (see Section 2.1.2) (**Figure 9**). It must be admitted that current spikes were registered while no bias was applied to the sample. However, the electric current observed by SPM can be associated with increase of concentration of photo induced carriers [93, 94]. Parasitic electrically induced potential can also lead to adverse stimulation of carriers. Since laser beam falling onto the SPM cantilever near the probe can over-illuminate the measured NW then both of these mechanisms can lead to observation of electrical spots during C-AFM spectroscopy or mapping. These influences can be overcome with adequate grounding and performing the experiments in dark conditions [93, 94].

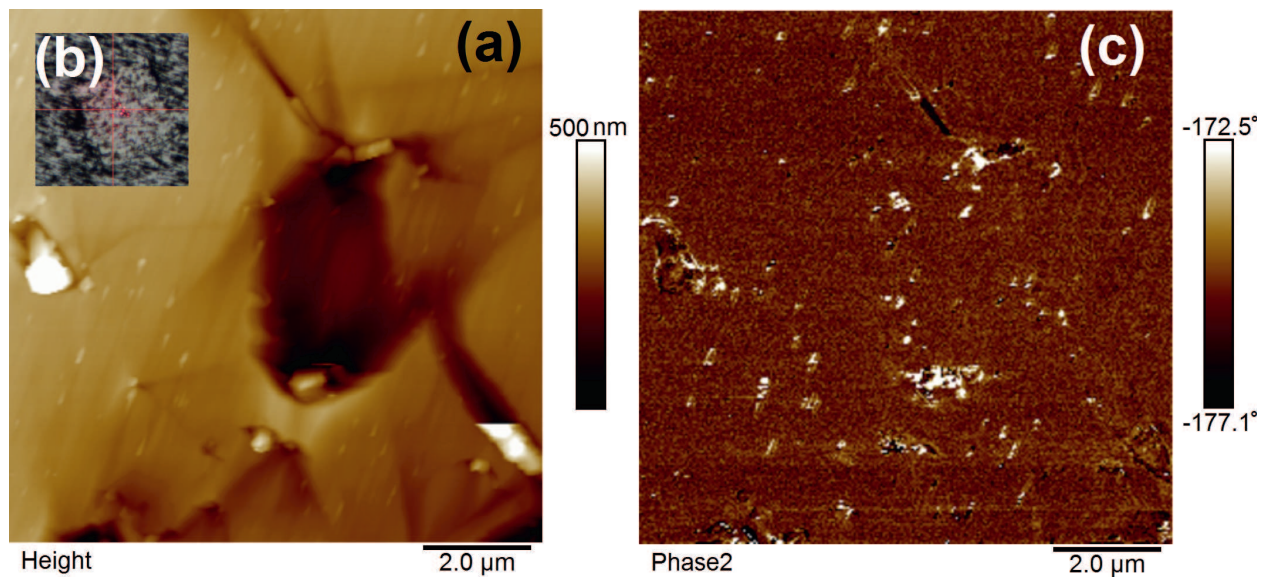


**Figure 8.** (a) 2D topography of a field with stumps left from an array of wurtzite GaAs NWs. (b) Optical image  $100 \times 100 \mu\text{m}$  representing square shaped field left after the breakage of vertical wurtzite GaAs NWs. (c) 2D image with a map of phase of the oscillations in lateral direction for a field with wurtzite GaAs stumps seen on (a) image. White spots indicate areas with higher amplitude indicating individual stumps.

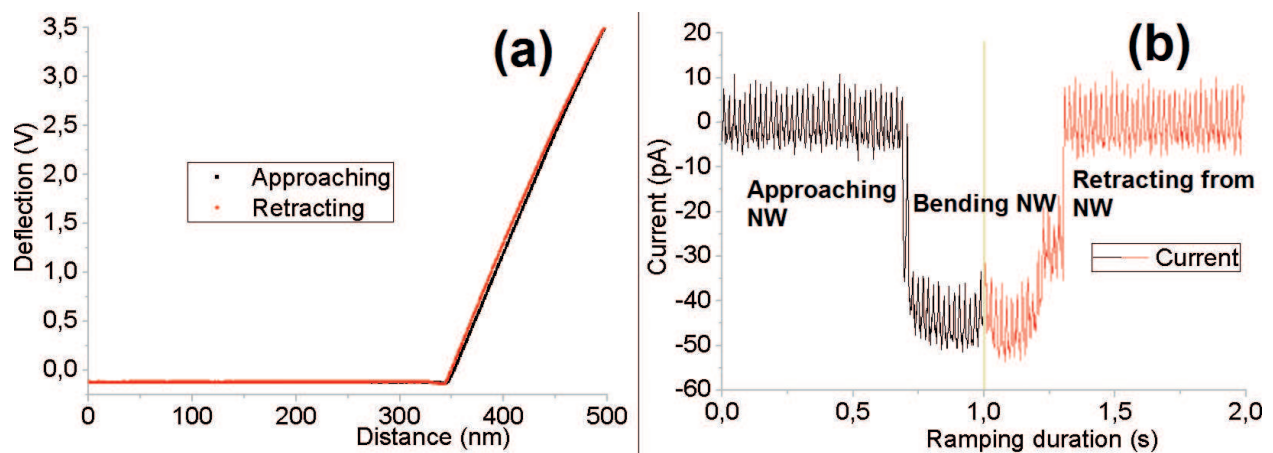


**Figure 9.** (a) Plot of  $F(z)$  for approaching and retracting from the sample where wurtzite NW was bended. (b) Current-time spectra  $I(t)$  registered during the bending of wurtzite GaAs NW.

Additionally, since these measurements are performed during almost seconds (while the value of current is considerably stable), it is potentially possible to evaluate the charge transferred  $q[\text{C}]$  and power  $P[\text{pW}]$ . This gives path to evaluation of performance of piezotronic devices with help of SPM by assessment of single NWs.

#### 4.2.2. Mapping of electrical current in NWs induced by controlled mechanical bending

Mapping of electric current in principle can help to visualize certain NWs producing higher values of electric current. See **Figure 10** taken under 0 V applied bias on WZ GaAs, where black spots are supposedly representing the current spikes measured in contact by SPM probe and generated due

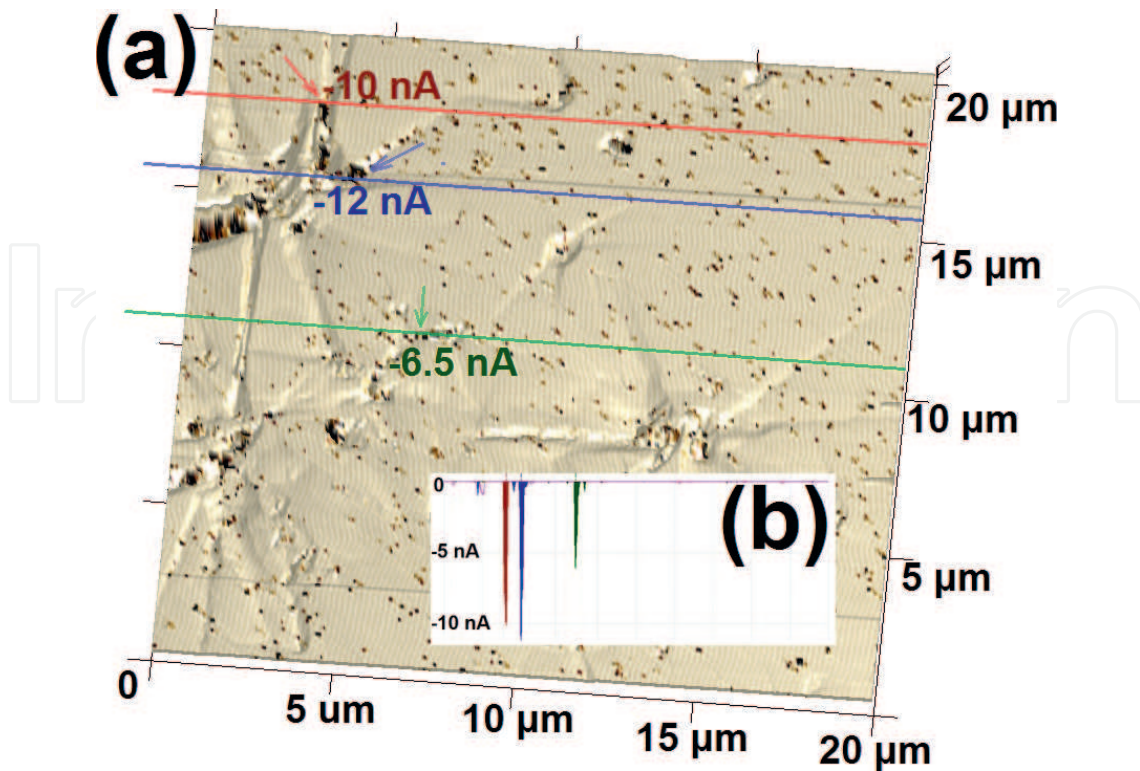


**Figure 10.** (a) 3D topography model of surface covered by stumps of wurtzite GaAs NWs seen as black spots due to overlaying of electric current map onto 3D topography. (b) Comparison of profiles of electric current taken for spots with highest electric current on from (a) image.

to mechanical stress of piezo responsive WZ GaAs material. This might indicate statistics about level of fabrication defects and overall quality of an array. Unfortunately, this approach is highly dependent from definite recognition of properties of energy barriers involved. Both Schottky barrier at the top part of NW and diffusion barrier at the bottom of NW (existing if materials of NW and substrate are different, e.g., Si and GaAs) can affect the result. In addition, triboelectricity can be an adverse factor during mapping of mechanical oscillations and it is aggravated for mapping in comparison with spectroscopy. Thus, triboelectric effect elaborates calculation of the input of piezo current and further evaluation of direct piezo coefficient of NW in nonvertical axis.

Shift of electric potential, which is registered as piezo response of the NWs' material, is suggested to be the result of redistribution of charge carriers inside NWs during their scanning/bending. Correspondingly, electric current that can be measured for piezoelectric NWs in PeakForce Tuna microscopy should indicate transfer of above-mentioned electric charges, i.e., electric current. Order of magnitude for such current is approximately few nanoamperes (**Figure 10b**). In addition, it can be possible to recalculate the current into potential, if resistance of the system is known. Unfortunately, heterojunction at the contact area between NW and a substrate obscures the transport mechanisms in such NWs. Revealing of mechanism of generation of electric current requires a separate comprehensive methodical study. This study should be performed on NWs with negligible energy barrier at its bottom contact with a substrate.

When aforementioned methodical difficulties will be overcome, a map of current density generated from each individual NW from an array would be visualized. In this respect, it

should be considered that force of push onto the NWs affects the value of electric potential induced in NWs. At the same time, altering rate of a setpoint force regulates the value of electric current produced by NW-based nanogenerators. Integral of current from single NW in time by its physical meaning defines the charge transferred into the SPM probe and recorded by SPM controller. Moreover, current from an array of NWs can be summed. Anticipated current output from an array containing plenty of NWs can be substantial for functioning of NW-based devices and can be characterized by current per certain area of an energy source [ $A/cm^2$ ]. Applicability of latter approach needs to be approved by experiments with properly arranged massive electrode grown above an array. Therefore, we can conclude that local methods still need to be strengthened by massive methods of research of NWs. The proposed concept of registering the piezo current presented here has debatable arguments but provides a room for improvements. If it would be realized in near future, it seems prolific for quick and accurate estimation of electricity generated by piezoelectric materials and NWs.

## 5. Conclusion

To summarize, nine types of experiments were described in this chapter with associated advantages and drawbacks of the SPM techniques. Different types of SPM probes paired as sharp/dull and flexible/stiff were specified for certain experiments with NWs. Congregation of methodical information was motivated toward better understanding of opportunities of microscopic techniques for studies of NWs. Comprehensive usage of these techniques depends on measuring systems available for certain research groups interested in study of NWs. While SPM systems continuously develop in latest decades, we emphasize that SPM is essentially useful, precise, and versatile tool for abovementioned purposes when properly operated. SPM allows studying electrical, mechanical, piezo properties, in addition to magnetic and optical properties, biocompatibility for medicine, chemical reactivity, etc.

In the course of our SPM research work, few significant findings were obtained in materials science. GaP should be preferably chosen as passivation material for GaAs NWs, while AlGaAs appeared also beneficial. Second, transparent protective medium of  $SiO_2$  has a complex influence onto conductive properties of NWs, i.e., energy barrier is reduced for unpassivated NWs, while it is strengthened for GaP-passivated NWs. These results were first obtained due to possibilities of SPM force control. Additionally, few methodical improvements were proposed. In the field of mechanics, the original mapping procedure of studies of tapered 10 nm thin NWs fixed at one end has been established. This allowed to first measurement of Young's modulus of wurtzite InP material, which exists recently only in nanothin state, i.e., solely in NWs. Therefore, it is a remarkable example of gathering a promising exotic nanomaterial and the only technique that can correctly describe its properties. Moreover, few original SPM experiments were proposed for comprehensive characterization of piezo properties of piezoelectric NWs in the field of electromechanics. Individual wurtzite GaAs NWs were experimentally investigated on the basis of proposed methodical electromechanical concepts. Lastly, studies of electrical conductivity of as-grown NWs are possible only with SPM. We developed the methodology of examination of as-grown vertical NWs and analysis of their I-V curves. The presented approach does not require an objectionable stage of the breakage of the

NWs followed by their fixation in horizontal lithographic MSM pattern for analyses as was done previously by other authors.

Considering the further outlook of SPM methods in studies of NWs, described approaches can be partly adapted to nonsemiconductor classes of materials, e.g., metals, polymers, insulators, ceramics, carbon ribbons, etc. Modern computational tools with proper procedures can assist standard microscope stations in realization of fast measurements and data recognition. Furthermore, components of SPM and experimental practices tend to be developed to an automated stage, resulting in even more powerful technique for studying versatile one-dimensional structures. Utilization of SPM allows obtaining of vital information about NWs, their individual and even local properties, which helps to better understanding of properties of an array of NWs and to design future devices based on NWs.

## Acknowledgements

Authors wish to thank a research group in Department of Micro and Nanosciences, Micronova, operating in Aalto University, Finland for fabrication and SEM visualization of vertical, horizontal and inclined NWs presented in Sections 2 and 3. Additionally, we thank the group of Laboratory of Nanoelectronics from St. Petersburg Academic University, St. Petersburg, Russia for growth and TEM visualization of piezo responsive GaAs NWs. PG thanks Dr. Prokhor Alekseev for thorough discussions providing significant contribution to the final version of the manuscript, Alina Lomenkova for help with graphical data analysis and Andrey Shubin from ScanSens GmbH for assistance with tungsten semicarbide probes. This work was supported by EU project Horizon2020-MSCA-RISE-691010 Hunter.

## Author details

Pavel Geydt<sup>1\*</sup>, Mikhail S. Dunaevskiy<sup>2</sup> and Erkki Lähderanta<sup>1</sup>

\*Address all correspondence to: pavel.geydt@lut.fi

1 Lappeenranta University of Technology, Lappeenranta, Finland

2 Ioffe Institute, St. Petersburg, Russia

## References

- [1] Xia Y, Yang P, Sun Y, Wu Y, Mayers B, Gates B, Yin Y, Kim F, Yan H. One-dimensional nanostructures: Synthesis, characterization, and applications. *Advances Materials*. 2003;**15**(5):353–389. DOI: 10.1002/adma.200390087

- [2] Dasgupta NP, Sun J, Liu C, Brittman S, Andrews SC, Lim J, Gao H, Yan R, Yang P. 25th anniversary article: Semiconductor nanowires – synthesis, characterization, and applications. *Advances Materials*. 2004;**26**(14):2137–2184. DOI: 10.1002/adma.201305929
- [3] Hochbaum AI, Yang P. Semiconductor nanowires for energy conversion. *Chemical Reviews*. 2010;**110**(1):527–546. DOI: 10.1021/cr900075v
- [4] Lu W, Xiang J, editors. *Semiconductor Nanowires: From Next-Generation Electronics to Sustainable Energy*. London, United Kingdom: RSC Publishing; 2015. p. 448. DOI: 10.1039/9781782625209
- [5] Arbiol J, Xiong Q, editors. *Semiconductor Nanowires: Materials, Synthesis, Characterization and Applications*. 1st ed. United Kingdom: Woodhead Publishing; 2015. p. 572. DOI: 10.1016/B978-1-78242-253-2.01001-X
- [6] Prete P, editor. *Nanowires*. Croatia: InTech; 2010. p. 428. DOI: 10.5772/3457
- [7] Zhang Z, Yao K, Liu Y, Jin C, Liang X, Chen Q, Peng L-M. Quantitative analysis of current–voltage characteristics of semiconducting nanowires: Decoupling of contact effects. *Advanced Functional Materials*. 2007;**17**:2478–2489. DOI: 10.1002/adfm.200600475
- [8] Arzt E. Size effects in materials due to microstructural and dimensional constraints: A comparative review. *Acta Materials*. 1998;**46**(16):5611–5626. DOI: 10.1016/S1359-6454(98)00231-6
- [9] Duan X, Huang Y, Cui Y, Wang J, Lieber CM. Indium phosphide nanowires as building blocks for nanoscale electronic and optoelectronic devices. *Nature*. 2001;**409**:66–69. DOI: 10.1038/35051047
- [10] Wang ZL, Song J. Piezoelectric nanogenerators based on zinc oxide nanowire arrays. *Science*. 2006;**312**(5771):242–246. DOI: 10.1126/science.1124005
- [11] Holm JV, Jørgensen HI, Krogstrup P, Nygård J, Liu H, Aagesen M. Surface-passivated GaAsP single-nanowire solar cells exceeding 10% efficiency grown on silicon. *Nature communications*. 2013;**4**(1498):1–5. DOI: 10.1038/ncomms2510
- [12] Cui Y, Wei Q, Park H, Lieber CM. Nanowire nanosensors for highly sensitive and selective detection of biological and chemical species. *Science*. 2001;**293**(5533):1289–1292. DOI: 10.1126/science.1062711
- [13] Wan Q, Li QH, Chen YJ, Wang TH, He XL, Li JP, Lin CL. Fabrication and ethanol sensing characteristics of ZnO nanowire gas sensors. *Applied Physics Letters*. 2004;**84**(18):3654–3656. DOI: 10.1063/1.1738932
- [14] Patolsky F, Lieber CM. Nanowire nanosensors. *Materials Today*. 2005;**8**(4):20–28. DOI: 10.1016/S1369-7021(05)00791-1
- [15] Lu W, Xie P, Lieber CM. Nanowire transistor performance limits and applications. *IEEE Transactions on Electron Devices*. 2008;**55**(11):2859–2876. DOI: 10.1109/TED.2008.2005158

- [16] Husain A, Hone J, Postma HWC, Huang XMH, Drake T, Barbic M, Scherer A, Roukes ML. Nanowire-based very-high-frequency electromechanical resonator. *Applied Physics Letters*. 2003;**83**(6):1240–1242. DOI: 10.1063/1.1601311
- [17] Feng XL, He R, Yang P, Roukes ML. Very high frequency silicon nanowire electromechanical resonators. *Nano Letters*. 2007;**7**(7):1953–1959. DOI: 10.1021/nl0706695
- [18] Binnig G, Quate CF, Gerber C. Atomic force microscope. *Physical Review Letters*. 1986;**56**:930–933. DOI: 10.1103/PhysRevLett.56.930
- [19] Giessibl FJ. Advances in atomic force microscopy. *Reviews of Modern Physics*. 2003;**75**:949–983. DOI: 10.1103/RevModPhys.75.949
- [20] Bhushan B, Fuchs H, editors. *Applied Scanning Probe Methods II—Scanning Probe Microscopy Techniques*. 1st ed. Germany: Springer-Verlag Berlin Heidelberg; 2006. p. 420. DOI: 10.1007/b139097
- [21] Marszalek PE, Greenleaf WJ, Li H, Oberhauser AF, Fernandez JM. Atomic force microscopy captures quantized plastic deformation in gold nanowires. *Proceedings of the National Academy of Sciences USA*. 2000;**97**(12):6782–6786. DOI: <https://www.ncbi.nlm.nih.gov/pmc/articles/PMC18594/>
- [22] Dobrokhotov VV, Yazdanpanah MM, Pabba S, Safir A, Cohn RW. Visual force sensing with flexible nanowire buckling springs. *Nanotechnology*. 2007;**19**(3):035502. DOI: 10.1088/0957-4484/19/03/035502
- [23] Wu C-H, Yeh N. Electrical properties and photoresponses of silicon nanowires with selective anchored gold nanoparticles via scanning probe bond breaking nanolithography. *Japanese Journal of Applied Physics*. 2009;**48**(4S): 04C152. DOI: 10.1143/JJAP.48.04C152
- [24] Sahin O. *Harmonic Force Microscope: A New Tool for Biomolecular Identification and Material Characterization Based on Nanomechanical Measurements [dissertation]*. USA: Stanford University; 2005. p. 113. Available from: <https://searchworks.stanford.edu/view/6212100>
- [25] Beinik I. *Electrical Characterization of Semiconductor Nanostructures by Conductive Probe Based Atomic Force Microscopy Techniques [dissertation]*. Austria: Montanuniversität Leoben; 2011. p. 118. Available from: <http://www.unileoben.ac.at/images/stories/Bibliothek/edoc/AC08511205n01vt.pdf>
- [26] Sadewasser S, Glatzel T, editors. *Kelvin Probe Force Microscopy—Measuring and Compensating Electrostatic Forces*. Germany: Springer; 2012. 334 p. DOI: 10.1007/978-3-642-22566-6
- [27] Teichert C, Beinik I. Conductive atomic-force microscopy investigation of nanostructures in microelectronics. In: Bhushan B, editor. *Scanning Probe Microscopy in Nanoscience and Nanotechnology 2*. Germany: Springer Berlin Heidelberg; 2010. pp. 691–721. DOI: 10.1007/978-3-642-10497-8\_23

- [28] Wang ZL. Nanopiezotronics. *Advanced Materials*. 2007;**19**(6):889–892. DOI: 10.1002/adma.200602918
- [29] Nakayama Y, Pauzauskis PJ, Radenovic A, Onorato RM, Saykally RJ, Liphardt J, Yang P. Tunable nanowire nonlinear optical probe. *Nature*. 2007;**447**:1098–1101. DOI: 10.1038/nature05921
- [30] Rossi N, Braakman FR, Cadeddu D, Vasyukov D, Tütüncüoğlu G, i Morral AF, Poggio M. Vectorial scanning force microscopy using a nanowire sensor. *Nature Nanotechnology*. 2017;**12**(2):150–155. DOI: 10.1038/nnano.2016.189
- [31] US Patent 8484756 B2. Bertness KA, Sanford NA, Kabos P, Wallis TM. Tip-Mounted Nanowire Light Source Instrumentation [Internet]. 2011. Available from: <https://www.google.com/patents/US8484756> [Accessed: 01.02.2017]
- [32] Yang G, Tang J, Kato S, Zhang Q, Qin LC, Woodson M, Liu J, Kim JW, Littlehei PT, Park C, Zhouless O. Magnetic nanowire based high resolution magnetic force microscope probes. *Applied Physics Letters*. 2005;**87**(12):123507. DOI: 10.1063/1.2043237
- [33] Park JJ, Reddy M, Stadler BJH, Flatau AB. Hysteresis measurement of individual multi-layered Fe-Ga/Cu nanowires using magnetic force microscopy. *Journal of Applied Physics*. 2013;**113**(17):17A331. DOI: 10.1063/1.4795818
- [34] Tabasum MR, Zighem F, Medina JDLT, Encinas A, Piraux L, Nysten B. Magnetic force microscopy investigation of arrays of nickel nanowires and nanotubes. *Nanotechnology*. 2014;**25**(24):245707. DOI: 10.1088/0957-4484/25/24/245707
- [35] Béron F, dos Santos MVP, de Carvalho PG, Moura KO, Arzuza LCC, Pirota KR. How to characterize cylindrical magnetic nanowires. In: Khan M, editor. *Magnetic Materials*. Croatia: InTech; 2016. pp. 41–69. DOI: 10.5772/63482
- [36] Dresselhaus MS, Lin Y-M, Rabin O, Black MR, Kong J, Dresselhaus G. Nanowires. In: Bhushan B, editor. *Springer Handbook of Nanotechnology*. Germany: Springer Berlin Heidelberg; 2010. pp. 119–167. DOI: 10.1007/978-3-642-02525-9\_4
- [37] Yang P, Yan H, Mao S, Russo R, Johnson J, Saykally R, Morris N, Pham J, He R, Choi H-J. Controlled growth of ZnO nanowires and their optical properties. *Advanced Functional Materials*. 2002;**12**(5):323–331. DOI: 10.1002/1616-3028(20020517)12:5<323::AID-ADFM323>3.0.CO;2-G
- [38] Kim DC, Dheeraj DL, Fimland BO, Weman H. Polarization dependent photocurrent spectroscopy of single wurtzite GaAs/AlGaAs core-shell nanowires. *Applied Physics Letters*. 2013;**102**(14):142107. DOI: 10.1063/1.4801865
- [39] Zhang Y, Wu J, Aagesen M, Liu H. III–V nanowires and nanowire optoelectronic devices. *Journal Physics D: Applied Physics*. 2015;**48**(46):463001. DOI: 10.1088/0022-3727/48/46/463001
- [40] Mukdadi OM, Datta SK, Dunn ML. Acoustic-phonon dispersion in nanowires. *Journal of Applied Physics*. 2005;**97**(7):0743123. DOI: 10.1063/1.1871333

- [41] McGary PD, Tan L, Zou J, Stadler BJH, Downey PR, Flatau AB. Magnetic nanowires for acoustic sensors (invited). *Journal of Applied Physics*. 2006;**99**(8):08B310. DOI: 10.1063/1.2167332
- [42] Young ESK, Bouravleuv AD, Cirlin GE, Dhaka V, Lipsanen H, Tchernycheva M, Scherbakov AV, Platonov AV, Akimov AV, Kent AJ. Electrical detection of picosecond acoustic pulses in vertical transport devices with nanowires. *Applied Physics Letters*. 2014;**104**(6):062102. DOI: 10.1063/1.4864637
- [43] Xie Q-Y, Ju Z-Y, Tian H, Xue Q-T, Chen Y-Q, Tao L-Q, Mohammad MA, Zhang X-Y, Yangac Y, Ren T-L. A point acoustic device based on aluminum nanowires. *Nanoscale*. 2016;**8**:5516–5525. DOI: 10.1039/C5NR06999H
- [44] Hernández-Mínguez A, Möller M, Breuer S, Pfüller C, Somaschini C, Lazić S, Brandt O, García-Cristóbal A, de Lima Jr. MM, Cantarero A, Geelhaar L, Riechert H, Santos PV. Acoustically driven photon antibunching in nanowires. *Nano Letters*. 2012;**12**(1):252–258. DOI: 10.1021/nl203461m
- [45] Kargar F, Debnath B, Kakko J-P, Säynätjoki A, Lipsanen H, Nika DL, Lake RK, Balandin AA. Direct observation of confined acoustic phonon polarization branches in free-standing semiconductor nanowires. *Nature Communications*. 2016;**7**:13400. DOI: doi:10.1038/ncomms13400
- [46] Burt DP, Wilson NR, Weaver JMR, Dobson PS, Macpherson JV. Nanowire probes for high resolution combined Scanning electrochemical microscopy—atomic force microscopy. *Nano Letters*. 2005;**5**(4):639–643. DOI: 10.1021/nl050018d
- [47] Hersam MC, Hoole ACF, O’Shea SJ, Welland ME. Potentiometry and repair of electrically stressed nanowires using atomic force microscopy. *Applied Physics Letters*. 1998;**72**(8):915. DOI: 10.1063/1.120872
- [48] Trukhin VN, Buyskikh AS, Kaliteevskaya NA, Bourauleuv AD, Samoilov LL, Samsonenko YB, Cirlin GE, Kaliteevski MA, Gallant AJ. Terahertz generation by GaAs nanowires. *Applied Physics Letters*. 2013;**103**(7):072108. DOI: 10.1063/1.4818719
- [49] Miao X, Chabak K, Zhang C, Mohseni PK, Walker Jr D, Li X. High-speed planar GaAs nanowire arrays with  $f_{\max} > 75$  GHz by wafer-scale bottom-up growth. *Nano Letters*. 2015;**15**(5):2780–2786. DOI: 10.1021/nl503596j
- [50] Haggrén T. Nanowire Technology for Optoelectronic Applications [dissertation]. Finland: Aalto University; 2016. p. 76. DOI: <https://aaltodoc.aalto.fi/handle/123456789/21918>
- [51] Bruker Inc. Application Note #132—Simultaneous Electrical and Mechanical Property Mapping at the nanoscale with PeakForce TUNA [Internet]. 2011. Available from: [https://www.bruker.com/fileadmin/user\\_upload/8-PDF-Docs/SurfaceAnalysis/AFM/ApplicationNotes/AN132-RevA0-Simultaneous\\_Electrical\\_Mechanical\\_Property\\_Mapping\\_with\\_PeakForce\\_TUNA-AppNote.pdf](https://www.bruker.com/fileadmin/user_upload/8-PDF-Docs/SurfaceAnalysis/AFM/ApplicationNotes/AN132-RevA0-Simultaneous_Electrical_Mechanical_Property_Mapping_with_PeakForce_TUNA-AppNote.pdf) [Accessed: 01.02.2017]

- [52] Dubrovskii VG, Cirilin GE, Ustinov VM. Semiconductor nanowhiskers: Synthesis, properties, and applications. *Semiconductors+*. 2009;**43**(1539):1585–1628. DOI: 10.1134/S106378260912001X
- [53] Rojo MM, Calero OC, Lopeandia AF, Rodriguez-Viejob J, Martín-Gonzalez M. Review on measurement techniques of transport properties of nanowires. *Nanoscale*. 2013;**5**:11526–11544. DOI: 10.1039/C3NR03242F
- [54] Kaja K. Development of nano-probe techniques for work function assessment and application to materials for microelectronics [dissertation]. France: Université Joseph-Fourier-Grenoble; 2010. p. 221. DOI: <https://tel.archives-ouvertes.fr/tel-00515370/en>
- [55] Chia ACE. Electrical Characterization and Optimization of Gallium Arsenide Nanowire Ensemble Devices [dissertation]. Canada: McMaster University; 2013. p. 155. DOI: <https://macsphere.mcmaster.ca/handle/11375/13335>
- [56] LaPierre RR, Chia ACE, Gibson SJ, Haapamaki CM, Boulanger J, Yee R, Kuyanov P, Zhang J, Tajik N, Jewell N, Rahman KMA. III–V nanowire photovoltaics: Review of design for high efficiency. *Physica Status Solidi Rapid Research Letters*. 2013;**7**(10):815–830. DOI: 10.1002/pssr.201307109
- [57] van Dam D, van Hoof NJJ, Cui Y, van Veldhoven PJ, Bakkers EPAM, Gómez Rivas J, Haverkort JEM. High-efficiency nanowire solar cells with omnidirectionally enhanced absorption due to self-aligned indium-tin-oxide Mie scatterers. *American Chemical Society Nano* 2016;**10**:11414–11419. DOI: 10.1021/acsnano.6b06874
- [58] Malloroqui AD. Nanowire-Based Solar Cells: Device Design and Implementation [dissertation]. EPFL Lausanne: Switzerland; 2014. p. 108. DOI: <https://infoscience.epfl.ch/record/196411>
- [59] Giordano MA, Schmidt SR. Applications of contact mode AFM to manufacturing processes. In: Bhushan B, editor. *Scanning Probe Microscopy in Nanoscience and Nanotechnology 2*. Germany: Springer Berlin Heidelberg; 2011. pp. 867–914. DOI: 10.1007/978-3-642-03535-7\_25
- [60] Tajik N. Sulfur Passivation of III–V Semiconductor Nanowires [dissertation]. Canada: McMaster University; 2013. p. 132. DOI: <https://macsphere.mcmaster.ca/handle/11375/12834>
- [61] Werner F, Limbach F, Carsten M, Denker C, Malindretos J, Rizzi A. Electrical conductivity of InN nanowires and the influence of the native indium oxide formed at their surface. *Nano Letters*. 2009;**9**(4):1567–1571. DOI: 10.1021/nl8036799
- [62] Lin X, He X, Lu J, Gao L, Huan Q, Deng Z, Cheng Z, Shi D, Gao H. Manipulation and four-probe analysis of nanowires in UHV by application of four tunneling microscope tips: a new method for the investigation of electrical transport through nanowires. *Surface and Interface Analysis*. 2006;**38**(6):1096–1102. DOI: 10.1002/sia.2333

- [63] Timm R, Persson O, Engberg DLJ, Fian A, Webb JL, Wallentin J, Jönsson A, Borgström MT, Samuelson, Mikkelsen A. Current–voltage characterization of individual as-grown nanowires using a scanning tunneling microscope. *Nano Letters*. 2013;**13**(11):5182–5189. DOI: 10.1021/nl402570u
- [64] Lord AM, Walton AS, Maffei TG, Ward MB, Davies P, Wilks SP. ZnO nanowires with Au contacts characterised in the as-grown real device configuration using a local multi-probe method. *Nanotechnology*. 2014;**25**(42):425706. DOI: 10.1088/0957-4484/25/42/425706
- [65] Geydt P, Alekseev PA, Dunaevskiy M, Lähderanta E, Haggrén T, Kakko J-P, Lipsanen H. Observation of linear I–V curves on vertical GaAs nanowires with atomic force microscope. *Journal of Physics: Conference Series*. 2015;**661**(1):012031. DOI: 10.1088/1742-6596/661/1/012031P
- [66] Geydt P, Alekseev PA, Dunaevskiy MS, Haggrén T, Kakko J-P, Lähderanta E, Lipsanen H. Influence of surface passivation on electric properties of individual GaAs nanowires studied by current–voltage AFM measurements. *Lithuanian Journal of Physics*. 2016;**46**(2):92–101. DOI: 10.3952/physics.v56i2.3305
- [67] Ellis JA, Barnes PA. Current–voltage characteristics of a GaAs Schottky diode accounting for leakage paths. *Applied Physics Letters*. 1999;**76**(1):124. DOI: 10.1063/1.125677
- [68] Suyatin DB, Jain V, Neboľ'sin VA, Trägårdh J, Messing ME, Wagner JB, Persson O, Timm R, Mikkelsen A, Maximov I, Samuelson L, Pettersson H. Strong Schottky barrier reduction at Au-catalyst/GaAs-nanowire interfaces by electric dipole formation and fermi-level unpinning. *Nature Communications*. 2014;**5**(3221):1–8. DOI: 10.1038/ncomms4221
- [69] Darbandi A, Salehzadeh O, Kuyanov P, La Pierre RR, Watkins SP. Surface passivation of tellurium-doped GaAs nanowires by GaP: Effect on electrical conduction. *Journal of Applied Physics*. 2014;**115**(23):234305. DOI: 10.1063/1.4883960
- [70] Dementyev PA, Dunaevskii MS, Samsonenko YB, Cirilin GE, Titkov AN. Current-voltage characteristics of silicon-doped GaAs nanowhiskers with a protecting AlGaAs coating overgrown with an undoped GaAs layer. *Semiconductors+*. 2010;**44**(5):610–615. DOI: 10.1134/S1063782610050118
- [71] Morita S. Roadmap of Scanning Probe microscopy. 1st ed. Germany: Springer-Verlag Berlin Heidelberg; 2007. p. 201. DOI: 10.1007/978-3-540-34315-8
- [72] Melitz W, Shen J, Kummel AC, Lee S. Kelvin probe force microscopy and its application. *Surface Science Reports*. 2011;**66**(1):1–27. DOI: 10.1016/j.surfrep.2010.10.001
- [73] Li G, Mao B, Lan F, Liu L. Practical aspects of single-pass scan Kelvin probe force microscopy. *Review of Scientific Instruments* 2012;**83**(11):113701. DOI: 10.1063/1.4761922
- [74] Prokhor AA. Investigation of Charge and Electric Field Distribution in Nanostructures by Scanning Probe Microscopy (in Russian) [dissertation]. Russian Federation: LETI; 2013. p. 159. Available from: <http://fizmathim.com/issledovanie-raspredeleniya-zaryadov-i->

elektricheskikh-poley-v-pribornyh-nanostrukturah-metodami-skaniruyushey-zondovoy-m  
DOI: <http://search.rsl.ru/ru/record/01005535363>

- [75] Dunaevskiy M, Alekseev P, Girard P, Lashkul A, Lahderanta E, Titkov A. Analysis of the lateral resolution of electrostatic force gradient microscopy. *Journal of Applied Physics*. 2009;**112**(6):064112. DOI: 10.1063/1.4752430
- [76] Hong KM, Noolandi J, Street RA. Theory of radiative recombination by diffusion and tunneling in amorphous Si: H. *Physical Review B*. 1981;**23**(6):2967. DOI: 10.1103/PhysRevB.23.2967
- [77] He R, Gao D, Fan R, Hochbaum AI, Carraro C, Maboudian R, Yang P. Si Nanowire bridges in microtrenches: Integration of growth into device fabrication. *Advanced Materials*. 2005;**17**(17):2098–2102. DOI: 10.1002/adma.200401959
- [78] Yong Oh J, Park J-T, Jang H-J, Cho W-J, Islam MS. 3D-transistor array based on horizontally suspended silicon nano-bridges grown via a bottom-up technique. *Advanced Materials*. 2014;**26**(14):1929–1934. DOI: 10.1002/adma.201304245
- [79] Shi C, Luu DK, Yang Q, Liu J, Chen J, Ru C, Xie S, Luo J, Ge J, Sun Y. Recent advances in nanorobotic manipulation inside scanning electron microscopes. *Microsystems & Nanoengineering*. 2016;**2**(16024):1–16. DOI: 10.1038/micronano.2016.24
- [80] Qin S, Kim T-H, Wang Z, Li A-P. Nanomanipulation and nanofabrication with multi-probe scanning tunneling microscope: From individual atoms to nanowires. *Review of Scientific Instruments*. 2012;**83**(6):063704. DOI: 10.1063/1.4727878
- [81] Wang ZL, Gao RP, Pan ZW, Dai ZR. Nano-scale mechanics of nanotubes, nanowires, and nanobelts. *Advanced Engineering Materials*. 2001;**3**(9):657–661. DOI: 10.1002/1527-2648(200109)3:9<657::AID-ADEM657>3.0.CO;2-0
- [82] Barth S, Harnagea C, Mathur S, Rosei F. The elastic moduli of oriented tin oxide nanowires. *Nanotechnology*. 2009;**20**(11):115705. DOI: 10.1088/0957-4484/20/11/115705
- [83] Chen CQ, Shi Y, Zhang YS, Zhu J, Yan YJ. Size dependence of young's modulus in ZnO nanowires. *Physical Review Letters*. 2006;**96**:075505. DOI: 10.1103/PhysRevLett.96.075505
- [84] Wang B, Stevens E, Leu PW. Strong broadband absorption in GaAs nanocone and nanowire arrays for solar cells. *Optics Express*. 2014;**22**(S2):A386–395. DOI: 10.1364/OE.22.00A386
- [85] Alekseev PA, Dunaevskii MS, Stovpyaga AV, Lepsa M, Titkov AN. Measurement of Young's modulus of GaAs nanowires growing obliquely on a substrate. *Semiconductors+*. 2012;**46**(5):641–646. DOI: 10.1134/S106378261205003X
- [86] Geydt P, Dunaevskiy M, Alekseev P, Kakko J-P, Haggrén T, Lähderanta E, Lipsanen H. Direct measurement of elastic modulus of InP nanowires with Scanning probe microscopy in PeakForce QNM mode. *Journal of Physical: Conference Series*. 2016;**768**(1):012029. DOI: 10.1088/1742-6596/769/1/012029

- [87] Gere JM, Goodno BJ. *Mechanics of Materials*. 8th ed. Stamford, USA: Cengage Learning; 2013. p. 1098. DOI: <http://trove.nla.gov.au/version/185463313>
- [88] Wachtman Jr JB, Tefft WE, Lam Jr DG, Apstein CS. Exponential temperature dependence of Young's modulus for several oxides. *Physical Reviews*. 1961;**122**(6):1754. DOI: 10.1103/PhysRev.122.1754
- [89] Dokukin ME, Sokolov I. Quantitative mapping of the elastic modulus of soft materials with Harmonix and PeakForce QNM AFM modes. *Langmuir*. 2012;**8**(46):16060–16071. DOI: 10.1021/la302706b
- [90] Xu F, Qin Q, Mishra A, Gu Y, Zhu Y. Mechanical properties of ZnO nanowires under different loading modes. *Nano Research*. 2010;**3**(4):271–280. DOI: 10.1007/s12274-010-1030-4
- [91] Espinosa HD, Bernal RA, Minary-Jolandan M. A review of mechanical and electromechanical properties of piezoelectric nanowires. *Advanced Materials*. 2012;**24**(34):4656–4675. DOI: 10.1002/adma.201104810
- [92] Wang ZL. Triboelectric nanogenerators as new energy technology and self-powered sensors—principles, problems and perspectives. *Faraday Discuss*. 2014;**176**:447–458. DOI: 10.1039/C4FD00159A
- [93] Lin Y-F, Song J, Ding Y, Lu S-Y, Wang ZL. Alternating the output of a CdS nanowire nanogenerator by a white-light-stimulated optoelectronic effect. *Advanced Materials*. 2008;**20**:3127–3130. DOI: 10.1002/adma.200703236
- [94] Song J, Wang X, Liu J, Liu H, Li Y, Wang ZL. Piezoelectric potential output from ZnO nanowire functionalized with p-type oligomer. *Nano Letters*. 2008;**8**(1):203–207. DOI: 10.1021/nl072440v

IntechOpen